

Targeting and function of proteins mediating translation initiation in organelles of *Plasmodium falciparum*

Afreen Haider,¹ Stacey M. Allen,²
Katherine E. Jackson,² Stuart A. Ralph² and
Saman Habib^{1*}

¹Division of Molecular and Structural Biology,
CSIR-Central Drug Research Institute, Lucknow, India.
²Department of Biochemistry and Molecular Biology,
Bio21 Molecular Science and Biotechnology Institute,
The University of Melbourne, Melbourne, Vic. 3010,
Australia.

Summary

The malaria parasite *Plasmodium falciparum* has two translationally active organelles – the apicoplast and mitochondrion, which import nuclear-encoded translation factors to mediate protein synthesis. Initiation of translation is a complex step wherein initiation factors (IFs) act in a regulated manner to form an initiation complex. We identified putative organellar IFs and investigated the targeting, structure and function of IF1, IF2 and IF3 homologues encoded by the parasite nuclear genome. A single *Pf*IF1 is targeted to the apicoplast. Apart from its critical ribosomal interactions, *Pf*IF1 also exhibited nucleic-acid binding and melting activities and mediated transcription anti-termination. This suggests a prominent ancillary function for *Pf*IF1 in destabilisation of DNA and RNA hairpin loops encountered during transcription and translation of the A+T rich apicoplast genome. Of the three putative IF2 homologues, only one (*Pf*IF2a) was an organellar protein with mitochondrial localisation. We additionally identified an IF3 (*Pf*IF3a) that localised exclusively to the mitochondrion and another protein, *Pf*IF3b, that was apicoplast targeted. *Pf*IF3a exhibited ribosome anti-association activity, and monosome splitting by *Pf*IF3a was enhanced by ribosome recycling factor (*Pf*RRF2) and *Pf*EF-G_{Mit}. These results fill a gap in our understanding of organellar translation in *Plasmodium*, which is the site of action of several anti-malarial compounds.

Accepted 14 February, 2015. *For correspondence. E-mail saman.habib@gmail.com, saman_habib@cdri.res.in; Tel. (+91) 522 2772477; Fax (+91) 522 2771941.

© 2015 John Wiley & Sons Ltd

Introduction

Plasmodium falciparum, the causal agent of malaria, is responsible for at least half-a-million annual human deaths. With the threat of the current line of drugs losing their efficacy, the search for newer anti-malarial targets gains immense importance. Each *Plasmodium* cell harbors two endosymbiotic organelles – a single mitochondrion and a relict plastid called the apicoplast, which is found in nearly all apicomplexan parasites. These organelles are essential for parasite survival, and their prokaryotic ancestry offers opportunities for drug intervention (Vaidya and Mather, 2009; Botte *et al.*, 2012). Although the mitochondrion supplies energy and an electron transport chain to drive parasite biosynthetic pathways, the apicoplast is the site of biochemical pathways leading to synthesis of fatty acids, haem, isoprenoids and assembly of [Fe-S] clusters (Lim and McFadden, 2010). Among organelar housekeeping functions, the protein translation machinery has emerged as a major site for anti-malarial intervention. Both the mitochondrion and apicoplast are sites of active translation (Chaubey *et al.*, 2005; Pino *et al.*, 2010; Jackson *et al.*, 2011), which is known to be targeted by several prokaryotic translation inhibitors exhibiting anti-malarial effects (Dahl *et al.*, 2006; Goodman *et al.*, 2007; Dahl and Rosenthal, 2008; Gupta *et al.*, 2013a).

Among components of the translation machinery, the reduced 6 kb mitochondrial genome of *P. falciparum* encodes only a few highly fragmented ribosomal RNA (rRNA) genes (Feagin *et al.*, 2012). Thus, all translation factors and transfer RNAs (tRNA) must be imported into this organelle. There is evidence that the mitochondrion of the related apicomplexan *Toxoplasma gondii* imports tRNAs in the aminoacylated state (Pino *et al.*, 2010), thus precluding the need for importing tRNA synthetases. The 35 kb *Plasmodium* apicoplast genome encodes a set of translation machinery components, 23S and 16S rRNA, a subset of large and small subunit ribosomal proteins, 24 tRNAs, and elongation factor Tu; it must import all aminoacyl-tRNA synthetases, many ribosomal proteins and ribosome assembly factors and the remaining translation factors (Wilson and Williamson, 1997; Jackson *et al.*, 2011; Gupta *et al.*, 2014). Investigations thus far have focused on *Plasmodium* aminoacyl-tRNA synthetases,

translation elongation factors and ribosome recycling (Biswas *et al.*, 2011; Jackson *et al.*, 2011; Gupta *et al.*, 2013a,b; Khan *et al.*, 2013) with little information on the first step of protein synthesis, i.e. translation initiation. Translation initiation is a complex process wherein initiation factors (IFs) act in a regulated manner to form a ternary initiation complex (IC) (Boelens and Gualerzi, 2002). The IC is a prerequisite for successful initiation and comprises an aminoacylated initiator-tRNA base paired to the initiation codon on the protein-encoding mRNA at the P-site of the ribosome. As in prokaryotes, translation in organelles requires IFs IF1, IF2 and IF3 with mitochondrial translation doing away with the requirement of an independent IF1 (Gaur *et al.*, 2008; Yassin *et al.*, 2011a).

Bacterial IF1 and IF3 are small soluble proteins that act in a concerted manner to split the vacant run-off 70S ribosome particles to provide the 30S subunit required for a new round of translation. IF3, known as the ribosome anti-association factor, binds with high affinity to the 30S subunit and shifts the equilibrium towards dissociation of 70S (Grunberg-Manago *et al.*, 1975). Cryo-EM studies in *Thermus thermophilus* and *Escherichia coli* show that the binding of IF3 at intimate docking points between the ribosomal subunits is the basis for this activity (McCutcheon *et al.*, 1999; Julian *et al.*, 2011). During initiation, IF3 also offers tight regulation by codon and substrate selection. It confers proofreading capability by promoting dissociation of a non-initiator-tRNA from the P-site and stabilising the interaction of fMet-initiator tRNA (Gualerzi *et al.*, 1977; Hartz *et al.*, 1990; La Teana *et al.*, 1993). A similar destabilisation property of IF3 is utilised in its function in post-termination ribosome recycling where it splits 70S ribosomes in conjunction with IF1 or as an adjunct factor with the ribosome recycling factor (RRF) and elongation factor EF-G (Singh *et al.*, 2005; Pavlov *et al.*, 2008). These roles of IF3 are also reportedly conserved in mitochondria and plastids of eukaryotes (Sharma *et al.*, 2013). IF3 has two compact N- and C-terminal domains joined by a flexible linker (Biou *et al.*, 1995; Garcia *et al.*, 1995a,b; Christian and Spremulli, 2009). Although the N-domain lacks ribosome dissociation activity, the C-domain is sufficient to carry out this function (Petrelli *et al.*, 2001); mutations in the C-domain of IF-3 interfere with both its prime roles in translation initiation (Petrelli *et al.*, 2003).

IF1 belongs to the oligomer binding (OB) fold-containing family of proteins, some of which are RNA-binding proteins, e.g. aspartyl-tRNA synthetase, ribosomal protein S1 and cold shock protein CspA. Bacterial IF1 is capable of binding to both the small subunit and intact 70S ribosome through interaction with 16S rRNA (Sette *et al.*, 1997; Carter *et al.*, 2001). Quantitative chemical footprinting and X-ray crystallography demonstrated that IF1 binds at the A-site of the ribosome suggesting that it plays a role in

mediating initiation fidelity by blocking premature access of aa-tRNAs to the A-site and directing initiator tRNA to the P-site (Dahlquist and Puglisi, 2000; Carter *et al.*, 2001). However, its exact role is still unclear. IF1 modulates the recycling of IF2 on and off the 70S IC and enhances the ribosome dissociation activity of IF3 (Boelens and Gualerzi, 2002). IF1 has also been shown to be a nucleic acid chaperone (Schleich *et al.*, 1980; Croitoru *et al.*, 2006), a property that mediates its moonlighting function of transcription anti-termination (Phadtare *et al.*, 2007; Phadtare and Severinov, 2009).

IF2, the largest of the IFs, is a GTPase that recruits the charged fMet-initiator tRNA onto the 30S ribosomal IC. It stimulates subunit joining to make the 70S ribosomal complex with the simultaneous release of IF1 and IF3. This is followed by activation of the intrinsic GTPase activity of IF2 resulting in adjustment of fMet-initiator tRNA in the P-site. GTP hydrolysis by IF2 drives its own ejection from the complex (Antoun *et al.*, 2003). IF2 is divided into the less conserved flexible N-terminal domain (subdomains I, II and III), which has a minor role in subunit assembly and the C-terminal domain (subdomains IV–VI) which has greater sequence similarity than the N-terminal domain to IF2 from bacteria, eukaryotes and archaeabacteria (Laursen *et al.*, 2005). The critical conserved domains comprising the C-terminal domain are the G-subdomain (IV) that is the GTP binding/GTPase center and the C-domain (VI), which is further subdivided into C1 (VI-1) and C2 (VI-2) domains. The C2 sub-domain interacts with the fMet-initiator tRNA (Laursen *et al.*, 2005).

The translation machinery in *Plasmodium* organelles differs from bacteria and other known organelar systems. Mitochondrial and apicoplast ribosomes in the parasite are considerably reduced and divergent from ribosomes of bacteria or characterised organelle ribosomes from other organisms (Feagin, 1992; Gupta *et al.*, 2014) and *P. falciparum* mitochondrial translation seems to function without elongation factor Ts (Biswas *et al.*, 2011). Also, similar to *T. gondii*, the *Plasmodium* mitochondrion likely imports tRNAs in the aminoacylated state (Pino *et al.*, 2010). We address translation initiation in *Plasmodium* organelles by identifying putative IFs, determining their subcellular targeting, and investigating function. Our data further support the view that translation initiation in *Plasmodium* organelles deviates somewhat from previously characterised systems and identifies ancillary functions of apicoplast IF1 in regulation of transcription and translation of the organelle's A+T-rich genome.

Results

Putative translation IFs for P. falciparum organelles

Putative organelar IFs identified on the basis of similarity with bacterial IFs and analysis of N-terminal targeting

Table 1. Putative *P. falciparum* organellar translation initiation factors and prediction for targeting to apicoplast/mitochondrion.

Translation initiation factor	PlasmoDB ID (previous ID)	Targeting prediction			Predicted organellar target	Confirmed localisation	
		TargetP 1.1 ^a (signal peptide)	PlasmoAP ^b (signal/transit peptide)	PATS ^c	MitoProtII ^d		
IF1	PF3D7_1469000 (PF14_0658)	0.98	0/-	0.99	0.59	Apicoplast	Apicoplast
IF2a	PF3D7_1312400 (PF13_0069)	0.02	-/-	0.10	0.85	Mitochondrion	Mitochondrion
IF2b	PF3D7_0516600 (PF08_0830c)	0.92	++/++	0.99	0.96	Apicoplast	Cytosolic
IF2c	PF3D7_0827100 (PF08_0018)	0.08	-/+	0.08	0.14	?	Cytosolic
IF3a	PF3D7_0825200 (MAL8P1.27)	0.92	++/++	0.97	0.22	Apicoplast	Mitochondrion
IF3b	PF3D7_1034600 (PF10_0336)	0.06	-/+	0.06	0.67	?	Apicoplast

a. Target P1.1 predicts subcellular location of eukaryotic proteins.

b. PlasmoAP gives scores for signal and transit peptide prediction for apicoplast targeting (Foth *et al.*, 2003). PlasmoAP prediction for signal/transit peptide is shown with 'very likely', 'likely', 'undecided' and 'unlikely' predictions denoted by '++', '+', '0' and '-' respectively.

c. PATS predicts targeting to *P. falciparum* apicoplast (Zuegge *et al.*, 2001).

d. MitoProtII is a tool for prediction of mitochondrial targeting sequences (Claros and Vincens, 1996).

sequence are listed in Table 1. A single IF1 (PF3D7_1469000) exhibiting 17% identity with the *E. coli* factor and with a positive prediction for signal and transit peptide for apicoplast targeting is encoded by the parasite nuclear genome (Fig. 1A). IF1 has not been found in other mitochondria (Spencer and Spremulli, 2005), and a similar scenario is likely to exist in *Plasmodium*. PF3D7_1312400 and PF3D7_0827100 (with 10.3% and 14.8% identity with *E. coli* IF2 respectively) were shortlisted as putative mitochondrial targeted IF2s (Fig. S1; Fig. 2A). Psi-blast searches using organellar IF2 homologues from *Bos taurus*, *Saccharomyces cerevisiae*, *Guillardia theta* and *Cyanidioschyzon merolae* did not identify any additional putative IF2. Because an IF2 with clear apicoplast prediction was not found, a previously studied sporozoite protein MB2 (PF3D7_0516600), which is also homologous to IF2 (14.5% identity with *E. coli* IF2), was selected (Fig. S1). This sequence has a strong apicoplast targeting prediction (Table 1). All IF2s selected for validation of putative organellar transport have conserved GTP binding/GTPase domain of the pfam family. As only a single IF3 (IF3a, PF3D7_0825200) (15.1% identity with *E. coli* IF3) that was predicted to be apicoplast-targeted was initially identifiable, we used psi-blast to probe the *P. falciparum* genome database using *Schizosaccharomyces pombe* mitochondrial IF3. A putative IF3 (PF3D7_1034600, IF3b) that exhibited ~12.3% identity with the query sequence was thus identified as a putative organelle translation IF (Table 1). It is noteworthy that primary sequence similarity between all the *Plasmodium* IFs and their corresponding *E. coli* orthologues is relatively low; this is congruent with many of the other components of the organellar protein translation apparatus (Gupta *et al.*, 2014). Multiple sequence alignment of *P. falciparum* putative organellar IF1 and IF3 with homologues from other organisms showed conservation of critical functional domains

(Figs S2 and S3); alignments of the much longer IF2 homologues also showed conservation of the G- and C-domains (not shown).

The single nuclear-encoded IF1 is targeted to the apicoplast

*Pf*F1 carrying an N-terminal 6xHis tag was expressed as a recombinant protein in *E. coli* [Fig. 3A (i)]. Antibodies generated against the purified protein recognised a 16.7 kDa form (corresponding to *Pf*F1 retaining a transit peptide but with signal sequence removed) and a ~11 kDa band in the parasite lysate [Fig. 3A (ii)]; the latter is the size expected after cleavage of both predicted signal and transit peptide sequences.

Because anti-*Pf*F1 antibody gave unclear signals in immunofluorescence assays, subcellular localisation of *Pf*F1 was investigated by generating a C-terminal HA-tagged *Pf*F1 line. Transfectants were selected and expression of the HA-tagged protein was checked by western blotting. A band of ~21 kDa (expected size of *Pf*F1+HA tag retaining transit peptide) and a second band of ~15 kDa (expected size of mature processed *Pf*F1+HA tag) were observed in western blot (Fig. 3B). Immunofluorescence assays using anti-HA Ab and antibodies against the apicoplast marker acyl carrier protein (ACP) showed a clear overlap of the two signals demonstrating that *Pf*F1 is targeted to the apicoplast (Fig. 3C).

Only one of three putative IF2s is an organellar protein

The C-domain of *Pf*F2a (639–1128aa) was expressed as a 63 kDa fusion protein with an N-terminal 6xHis-tag [Fig. 4A (i)]. Antibodies raised against the protein recognised a ~110 kDa band in parasite lysate [Fig. 4A (ii)]. *Pf*F2a is predicted by TargetP1.1 (Emanuelsson *et al.*,

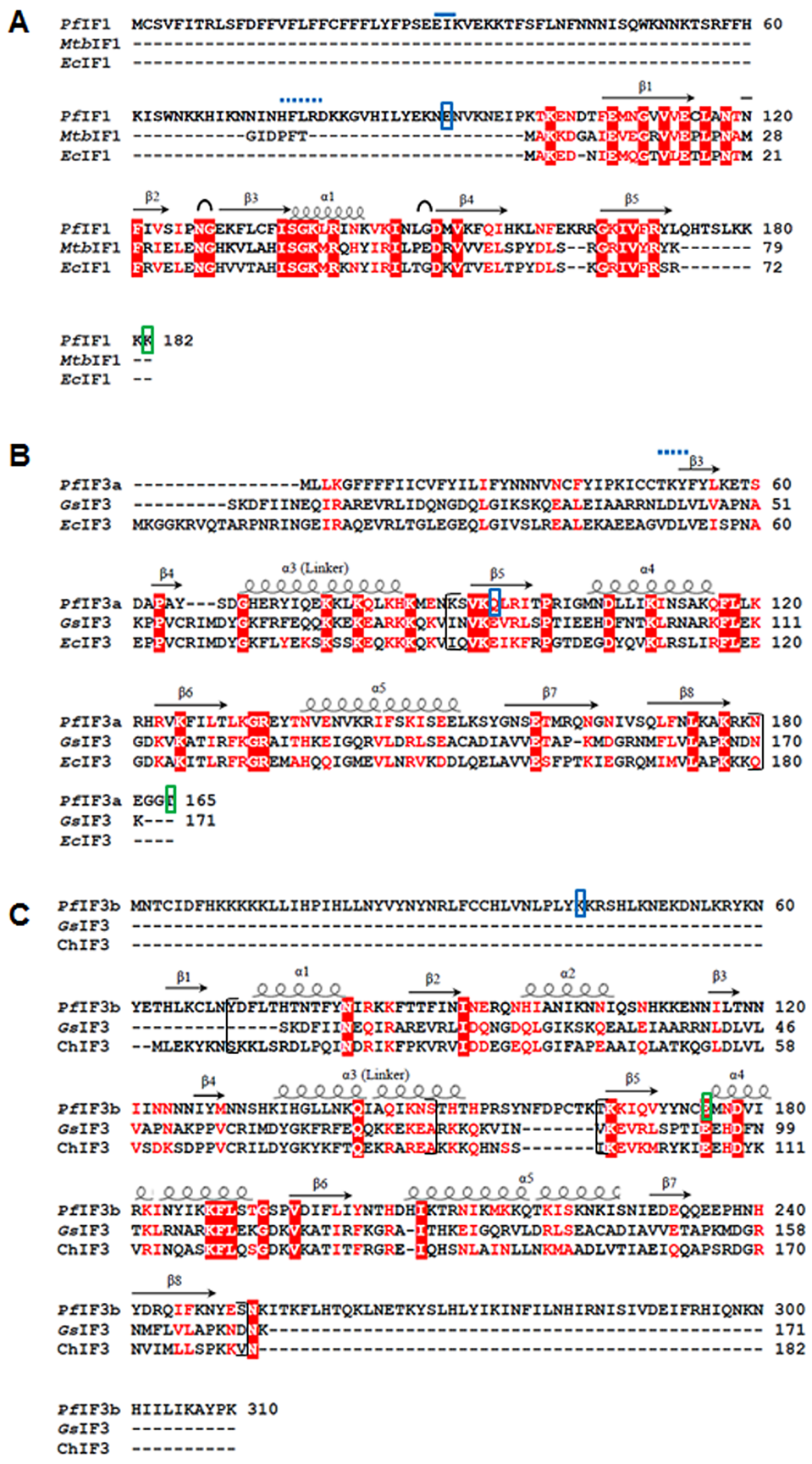


Fig. 1. ClustalW alignments of (A) *PfIF1*, (B) *PfIF3a* and (C) *PfIF3b* with bacterial or plastid homologues. Blue line in the clustalW alignments indicate signal cleavage site, blue dotted line marks the putative transit/mitochondrial leader cleavage site and blue and green boxes indicate the first and last amino acids of the recombinant proteins. Black brackets indicate regions of the two IF3 proteins that were modelled as shown in Fig. S2. Other structural assignments indicated in the alignments are based on Jpred3 predictions. *Pf*, *P. falciparum*; *Ch*, chloroplast of *Porphyra purpurea*; *Ec*, *E. coli*; *Gs*, *Geobacillus stearothermophilus*; *Mtb*, *Mycobacterium tuberculosis*.

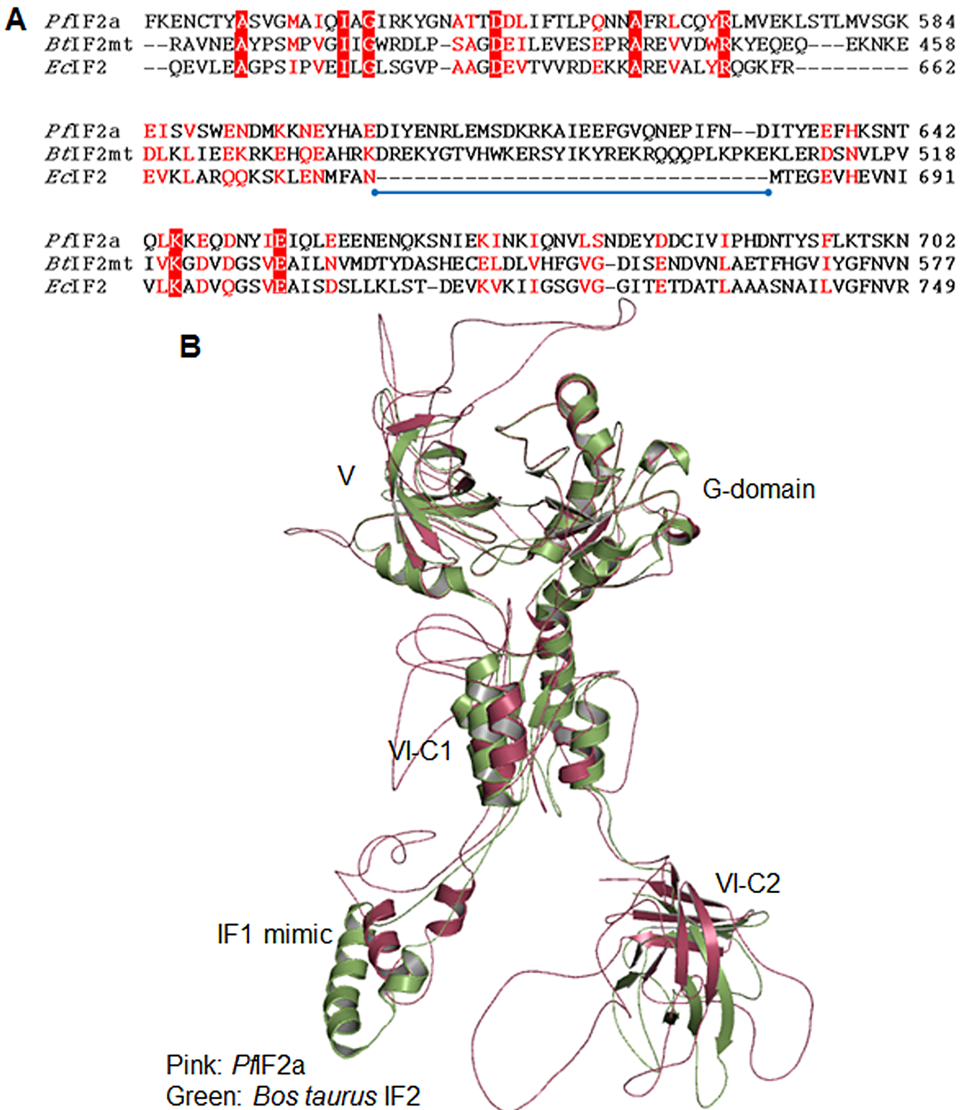


Fig. 2. A. ClustalW alignment revealing the insertion (IF1 mimic) between domains V and VI in the *PfIF2a* and *Bos taurus* IF2 sequences compared with *E. coli* IF2. B. Structure modelling of *PfIF2a* (pink) with *BtIF2* (green) as template.

2007) to have a long mitochondrial targeting leader of 89aa, which implies that the size of the mature organellar protein would be 114 kDa. Thus, the ~110 kDa band detected in western blot of the parasite lysate (Fig. 4A) is likely to represent processed mitochondrial *PfIF2a*. Anti-IF2a serum was used in immunofluorescence assays for subcellular localisation of *PfIF2a* (Fig. 4B). Clear overlap of the mitochondrial dye and *PfIF2a* signal was observed [Fig. 4B (i)]. No overlap was seen with the apicoplast marker *PfHU* that was detected using anti-*PfHU* Abs [Fig. 4B (ii)] indicating that *PfIF2a* localised exclusively in the *P. falciparum* mitochondrion.

The ability of mitochondrial *PfIF2a-C* to interact with initiator-tRNA that carried either formylated or unformylated methionine was investigated by EMSA using

E. coli Met-tRNA^{fMet} or fMet-tRNA^{fMet} as probes (Fig. 4C). *PfIF2a-C* interacted with initiator-tRNA, indicating that mitochondrial *PfIF2a* has conserved molecular determinants for initiator-tRNA recognition and binding. Detection of binding of *PfIF2a* with *E. coli* Lys-tRNA^{Lys} only at very high concentrations of the protein confirmed specificity of the *PfIF2a*-initiator tRNA interaction (Fig. 4C). Comparable K_D values for binding obtained with Met-tRNA^{fMet} and fMet-tRNA^{fMet} (Fig. 4D) suggested that *PfIF2a* recognises aminoacylated initiator-tRNA irrespective of its formylation status.

Generation of C-terminal HA-tagged transfected lines was attempted for localisation of *PfIF2b* and *PfIF2c*. Transfectants expressing the *PfIF2b-HA* fusion protein were obtained (Fig. S4A), but no *PfIF2c-HA* transfectants could

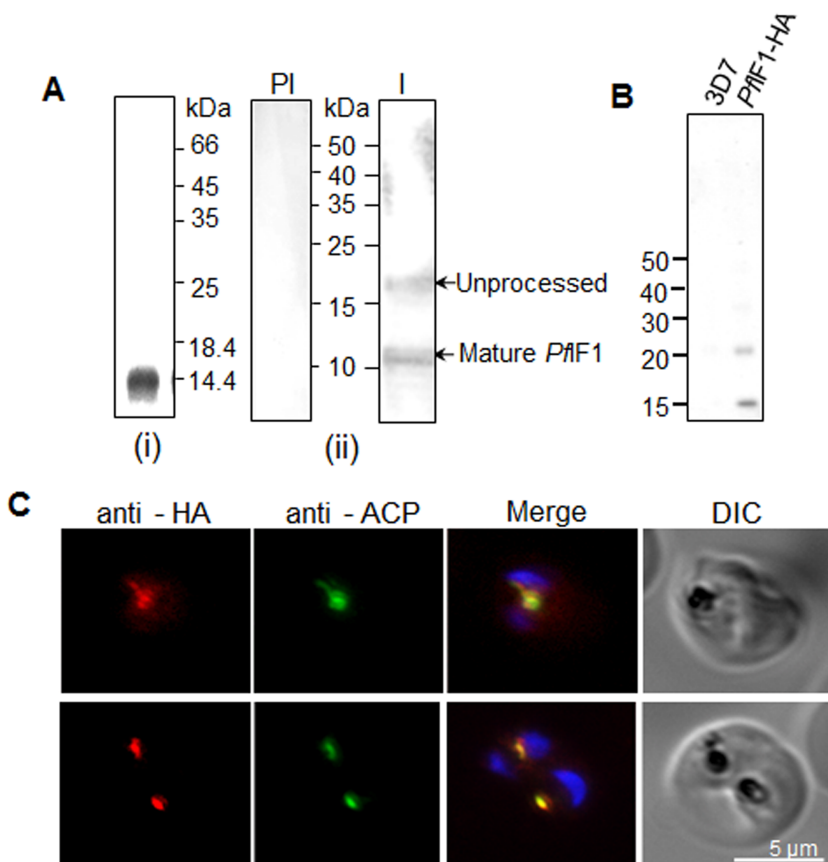


Fig. 3. Detection and localisation of *Pif1*.
 A. Coomassie-stained gel of purified recombinant *Pif1* (panel i) and western blot of parasite lysate from infected erythrocytes with IF1 detected using anti-IF1 serum (panel ii). PI, pre-immune serum; I, immune serum.
 B. Detection of IF1-HA fusion protein in the transfected line. Western blot with anti-HA Ab recognises an intact ~21 kDa (*Pif1*+HA tag) product and a ~15 kDa band representing the N-terminal processed protein.
 C. Immunofluorescence localisation of *Pif1*-HA using the anti-HA Ab and antibody against the apicoplast marker ACP. The two rows show different parasitised RBCs with complete overlap of *Pif1*-HA signal observed with apicoplast ACP. Nuclear DNA is stained with DAPI.

be selected. Therefore, the N-terminal sequence of *Pif2c* was cloned as a fusion with GFP for determination of subcellular targeting. Immunofluorescence assays for *Pif2b* showed cytosolic distribution with some punctate signals that did not colocalise with either the apicoplast or the mitochondrion (Fig. S4B). The *Pif2c* targeting sequence-GFP signal was also seen throughout the cytoplasm and the protein did not colocalise with either organelle marker (Fig. S4C). Thus, out of the three putative *Pif2s* examined, only *Pif2a* was localised to a parasite organelle and is a mitochondrial protein.

IF3a and IF3b are mitochondrial and apicoplast factors respectively

Because we were unable to express full-length *IF3a*, the predicted ribosomal binding domain (76–165aa) was expressed in fusion with a C-terminal 6xHis-tag to generate an ~15 kDa protein [Fig. 5A (i)]. Antibodies raised against the recombinant protein recognised an unprocessed form of 19 kDa and a mature protein of ~15 kDa in western blots of parasite lysate [Fig. 5A (ii)]. Anti-*Pif3a* serum was then used for subcellular localisation of the protein in immunofluorescence assays with infected erythrocytes. *Pif3a* signal distinctly colocalised with the mitochondrial marker dye [Fig. 5C (i) and (ii)] and did not exhibit

any overlap with the apicoplast marker protein HU [Fig. 5B (iii)]. These results indicate that *Pif3a* is a mitochondrial factor and that prediction for its apicoplast targeting (Table 1) is incorrect. The ~15 kDa band corresponding to the mature protein seen in parasite lysates suggests that the mitochondrial leader cleavage site is at around 35–39aa from the N-terminus (Fig. 1B).

A part of the gene encoding *Pif3b* (43–175aa) was expressed in *E. coli*. Most recombinant *Pif3b* partitioned in the insoluble fraction (Fig. S5A) and the small amount of soluble protein was very unstable. *Pif3b* inclusion bodies were used to raise antiserum in mice. Anti-*Pif3b* serum recognised a ~34 kDa band slightly below the expected size of the unprocessed protein (37 kDa) (Fig. S5B). In immunofluorescence assays using the anti-*Pif3b* serum, the *Pif3b* signal clearly colocalised with the apicoplast marker HU [Fig. 5C (i) and (ii)] and was distinct from the mitochondrial marker dye [Fig. 5C (iii)], thus identifying *Pif3b* as an apicoplast factor.

Structural modelling of organellar IFs

Molecular modelling of four IFs (*Pif1*, *Pif2a*, *Pif3a* and *Pif3b*) with confirmed localisation to parasite organelles was carried out. Apicoplast-targeted *Pif1* modelled on the crystal structure of *Mycobacterium tuberculosis* IF1

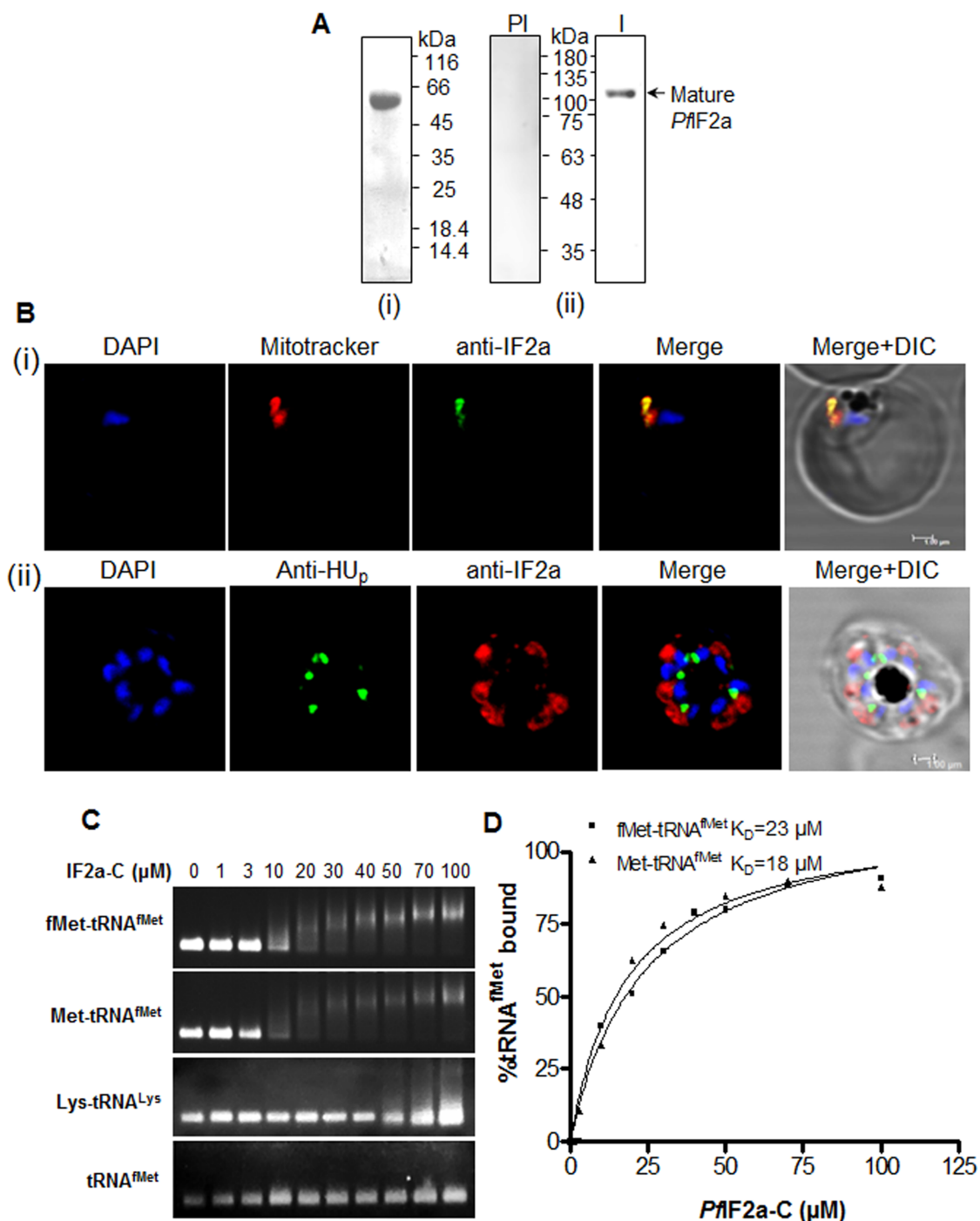


Fig. 4. Detection and localisation of *PifF2a* in *P. falciparum*-infected erythrocytes, and its interaction with initiator tRNA.

A. Coomassie-stained gel of purified recombinant *PifF2a*-C (panel i) and detection of *PifF2a* by western blot of parasite lysate using anti-*PifF2a*-C serum (panel ii).

B. Immunofluorescence assay (IFA) with anti-*PifF2a*-C serum and the mitochondrial dye Mitotracker Red CMXROS (panel i); IFA to detect the apicoplast marker protein *PfHUp* (using *PfHUp* antisera) and *PifF2a* (panel ii). Parasite nuclear DNA is stained with DAPI.

C and D. Binding of *PifF2a*-C with *E. coli* Met-tRNA^{fMet} and fMet-tRNA^{fMet} detected by EMSA in the presence of increasing concentrations of the protein. *E. coli* Lys-tRNA^{Lys} and uncharged tRNA^{fMet} were used as controls (D) K_D values for initiator-tRNA binding were calculated from data shown in (C).

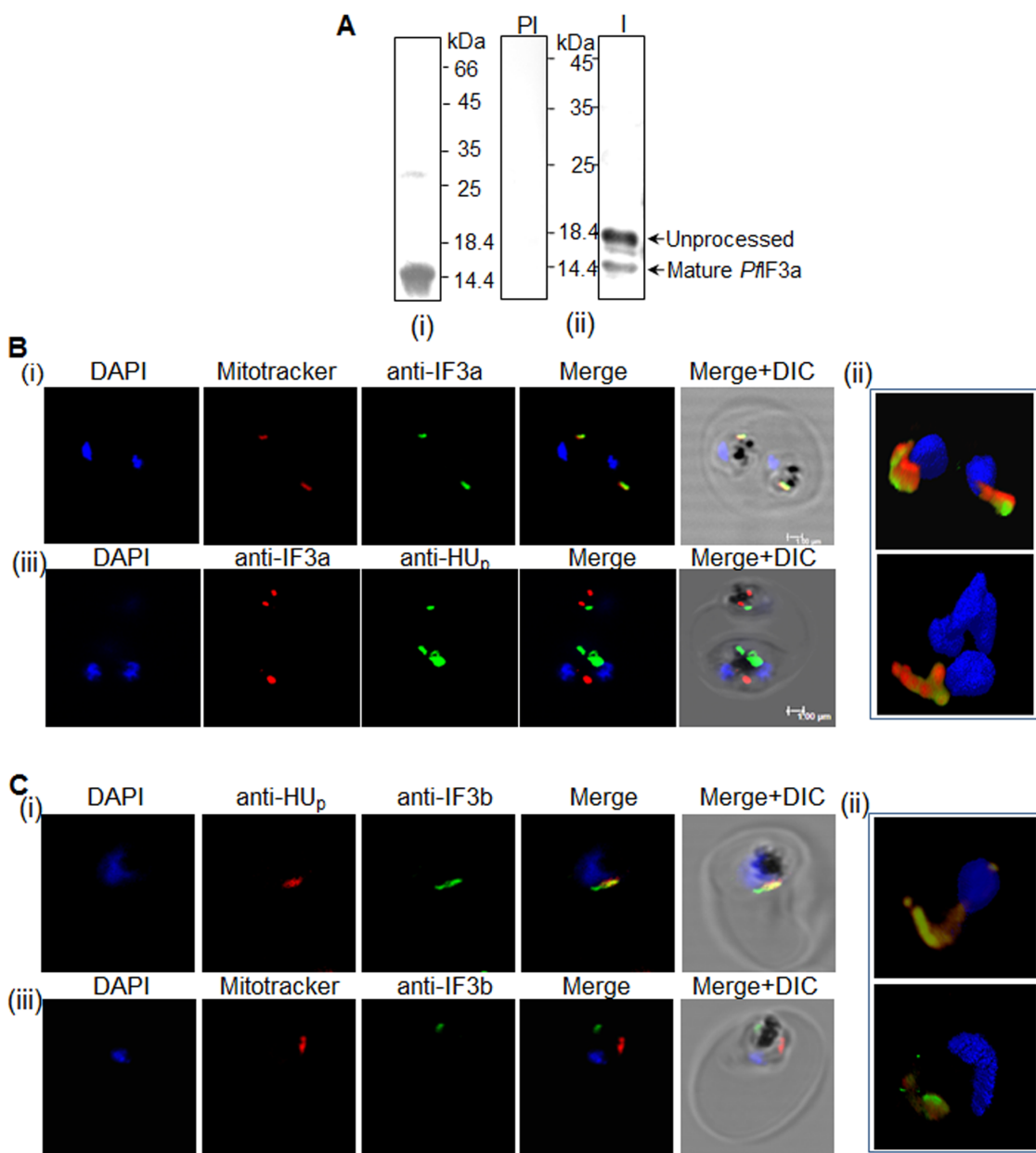


Fig. 5. Immunofluorescence localisation of *PifF3a* and *PifF3b*.

A. Coomassie-stained gel of purified recombinant *PifF3a* (panel i) and western blot of parasite lysate with *PifF3a* detected using anti-IF3a serum (panel ii).

B. Panel i, *P. falciparum*-infected erythrocytes stained with Mitotracker Red and probed with *PifF3a* antiserum; panel ii, 3-dimensional reconstruction after z-sectioning shows clear overlap of the *PifF3a* signal with the mitochondrion; panel iii, Absence of overlap of the *PifF3a* signal with apicoplast *PfHU*.

C. Panel i, parasitised erythrocytes probed with anti-IF3b and anti-HU_p anti-sera; panel ii, 3-dimensional reconstruction shows overlap of IF3b with apicoplast HU_p; panel iii, *PifF3b* signal does not overlap with Mitotracker Red. Nuclear DNA is stained with DAPI.

(Hatzopoulos and Mueller-Dieckmann, 2010) (Fig. S6A) showed conservation of the S1 domain of the oligomer-binding (OB) fold and a five-strand β-barrel with the loop between β strands 3 and 4 capping one end of the barrel. The *Plasmodium* IF1 has ~24aa and 9aa long extensions at the N- and C-terminus that could not be modelled. Even

though *PifF1* has low sequence identity to bacterial IF1, molecular modelling indicates structural resemblance suggesting functional conservation in *PifF1*.

Mitochondrion-targeted *PifF2a* was modelled on the cryo-EM structure of *B. taurus* IF2_{Mit} (Yassin *et al.*, 2011a). Mitochondrial IF2s have six structural domains that are

homologous to domains III-VI of bacterial IFs (Spencer and Spremulli, 2005). The region corresponding to domains I-II of bacterial IF2 is also not conserved in *PfIF2a*, with maximal similarity starting close to the G domain (domain IV) onwards (Fig. S1A). ClustalW alignment of *PfIF2a* with *BtIF2_{Mit}* and *EclF2* indicated the presence of two large insertions of 80aa (between domain IV and V) and 23aa (in domain VI-C2), and a 253aa long C-terminal extension in *PfIF2a* (Fig. S1A). The *PfIF2a* sequence also contains a 29aa insertion corresponding to the region that functions as an IF1 mimic in mitochondrial IF2s (Gaur et al., 2008; Yassin et al., 2011a) (Fig. 2A). Because the *BtIF2_{Mit}* structure starts from the G-domain, molecular modelling of the corresponding region of *PfIF2a* was carried out. Extensive fold conservation was evident in the IF2a model (Fig. 2B), although the insertions in *PfIF2a* could not be modelled and appear as loops. The 29aa insertion between domain V and VI positions at the same location as the 37aa long IF1 mimic sequence of *BtIF2_{Mit}* that protrudes into the A-site. In *PfIF2a*, this insertion models as a loop with two α -helices (Fig. 2B).

IF3 comprises two distinct IF3-N and -C domains that are proposed to be connected by an α -helical linker (Biou et al., 1995). *PfIF3a* has a truncated N-terminal domain with conservation only of the region encompassing the α -helical linker and two β -strands (Fig. 1B). *PfIF3a* primarily exhibits homology with the C-domain of bacterial IF3 and was thus modelled on the *Geobacillus stearothermophilus* IF3 C-domain (Biou et al., 1995). Extensive fold conservation in the two parallel α -helices packed against a mixed four β -strand sheet of *GslF3* C-domain and the corresponding stretch of *PfIF3a* was evident (Fig. S6B). Apicoplast-targeted *PfIF3b* is larger compared with mitochondrial *PfIF3a* and has both N- and C-domains with a connecting linker. Both domains model on the corresponding domains of *GslF3* (Fig. S6C) indicating structural conservation with bacterial IF3 despite low overall sequence identity.

PfIF1 and *PfIF3a* interact with ribosomes

The ability of *PfIF1* and *PfIF3a* to interact with surrogate *E. coli* ribosome 30S and 50S subunits was assayed by the filter-trap method. Both *PfIF1* and *PfIF3a* were retained on the filter only in the presence of the 30S subunit as seen in both Coomassie-stained gel and western blot with anti-His Ab (Fig. 6, lanes 5 and 7). *PfIF1* and *PfIF3a* passed through the filter in the absence of the ribosome and were not detected in the control lanes (Fig. 6, lanes 1 and 2). Glutathione-S-transferase (GST), used as control, did not bind to either subunit (Fig. S7). These results demonstrate that both apicoplast-targeted *PfIF1* and mitochondrial-targeted *PfIF3a* are capable of interacting with the small ribosomal subunit.

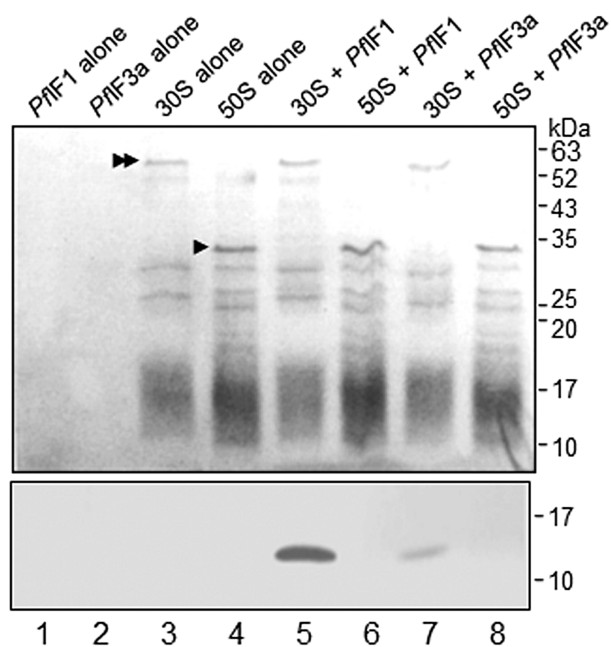


Fig. 6. Recombinant *PfIF1* and *PfIF3a* interact with the *E. coli* ribosome 30S subunit. Coomassie-stained gel (upper panel) and corresponding western blot with anti-His Ab (lower panel) showing retention of *PfIF1* and *PfIF3a* on the filter only in the presence of 30S *E. coli* subunit (lanes 5 and 7 respectively). Both proteins pass through the filter in the absence of the ribosome (lanes 1 and 2) and do not interact with the 50S subunit (lanes 6 and 8). Single and double arrows indicate Rpl2 and Rps1 proteins of the 50S and 30S subunits respectively.

PfIF3a exhibits ribosome anti-association activity and enhances monosome splitting by mitochondrial EF-G and RRF

IF3 inhibits the reassociation of ribosomal subunits. This anti-association activity of *PfIF3a* was assayed by using *E. coli* 70S ribosomes that were first split into the 50S and 30S subunits in low Mg²⁺ buffer. The subunits reassociated in the presence of high Mg²⁺ (Fig. 7A, control). However, reassociation into 70S was inhibited in the presence of both *EclF3* (Gupta et al., 2013b) and *PfIF3a* (Fig. 7A) indicating that the subunit anti-association activity, mediated by the binding of the factor to the 30S subunit, is conserved in *P. falciparum* mitochondrial IF3.

IF3 also has a role in recycling of ribosomes that is mediated by its subunit dissociation activity. The ability of *PfIF3a* to dissociate the 70S ribosomal unit (monosome) was tested in an *E. coli* monosome splitting assay. *PfIF3a* could split 70S monosomes into the constituent 50S and 30S subunits (Fig. 7B). The *P. falciparum* mitochondrial ribosome recycling factors RRF2 and EF-G_{Mit} have been shown to mediate monosome splitting in the presence of *EclF3* (Gupta et al., 2013b). The ribosome splitting activity of RRF2 and EF-G_{Mit} was also enhanced in the presence of mitochondrial *PfIF3a* (Fig. 7B), suggesting that ribo-

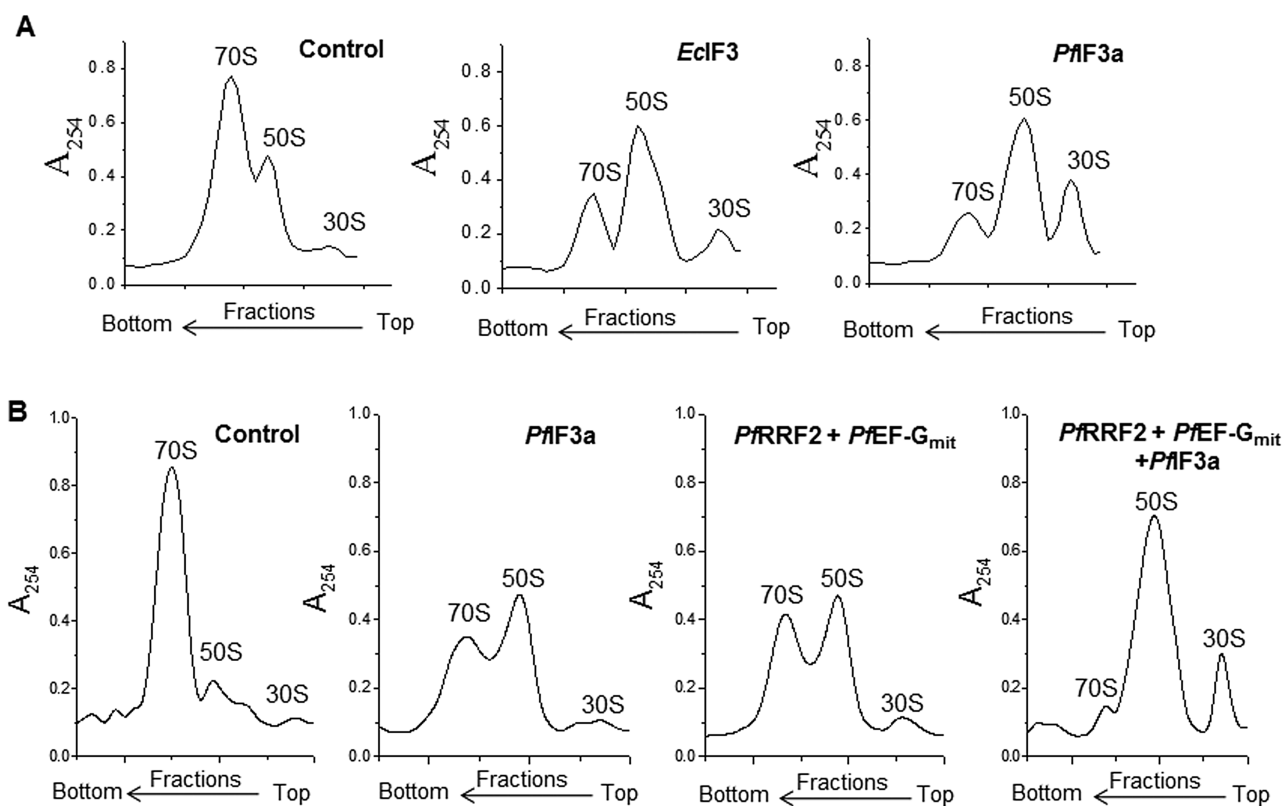


Fig. 7. Ribosome anti-association activity and monosome splitting by *Pif3a*.

A. The reassembly of *E. coli* split ribosomes is prevented in the presence of *Pif3a*, whose anti-association activity is comparable with that of *EclF3*. Split 50S and 30S subunits (in low Mg^{2+}) reassemble as 70S (in high Mg^{2+}) in the absence of IF3 (control).
B. *Pif3a* can split 70S monosomes into the constituent 50S and 30S subunits and enhanced ribosome splitting is observed in the presence of *PifEF-G_{mit}*, mitochondrial *PifRRF2*, and *Pif3a*.

some recycling in the parasite mitochondrion is mediated by the co-ordinated activity of RRF2, EF-G_{mit} and IF3a.

Apicoplast IF1 binds nucleic acids and has anti-termination activity

IF1 has an S1 domain that categorises it within the OB domain-containing family of proteins whose members include cold shock domain-containing proteins such as CspA and CspE of *E. coli*. The presence of this fold has been proposed to impart IF1 with an additional ability to serve as a nucleic acid chaperone, a property mediated by melting of nucleic acid secondary structures (Phadtare and Severinov, 2009). The ability of apicoplast *Pif1* to bind to nucleic acids was assayed by EMSA using a fluorophore (FAM)-labelled DNA probe. A DNA-protein shift was observed in the presence of increasing concentrations of *Pif1* (Fig. 8A), indicating the nucleic-acid binding capacity of the protein. Furthermore, the ability of *Pif1* to melt DNA was tested using a partially double-stranded *Invertbeacon* sequence with a 9 bp stem and 4nt 5'-overhang (Fig. 8B) that was exposed to cleavage by $KMnO_4$ probing in the presence or absence of *Pif1*.

Although only external exposed thymines were cleaved by $KMnO_4$ alone, an additional internal cleavage product was observed in the presence of *Pif1* (Fig. 8B) indicating DNA melting that results in exposure of an internal thymine in the presence of the protein.

In vitro DNA melting by *E. coli* CspE has been shown to correlate well with transcription anti-termination by the factor (Phadtare *et al.*, 2007). We thus tested transcription anti-termination by *Pif1* *in vivo*, using the *E. coli* strain RL211 (Weilbaecher *et al.*, 1994). The RL211 strain carries a chloramphenicol acetyltransferase (*cat*) gene preceded by a Rho-independent *trpL* terminator and is therefore sensitive to chloramphenicol. However, if transcription proceeds beyond the terminator, the *cat* gene is transcribed and cells become resistant to chloramphenicol [Fig. 8C (i)]. RL211 cells transformed with pQE30 or pQE30-*Pif1* grew equally well in the presence of ampicillin alone [Fig. 8C (i)]. Only RL211 cells transformed with the pQE30-*Pif1* expression plasmid were able to grow in the presence of chloramphenicol, whereas those transformed with pQE30 alone were chloramphenicol sensitive. The growth of transformed *E. coli* RL211 cells in the presence of ampicillin and chloramphenicol was also monitored over 24 hours, and

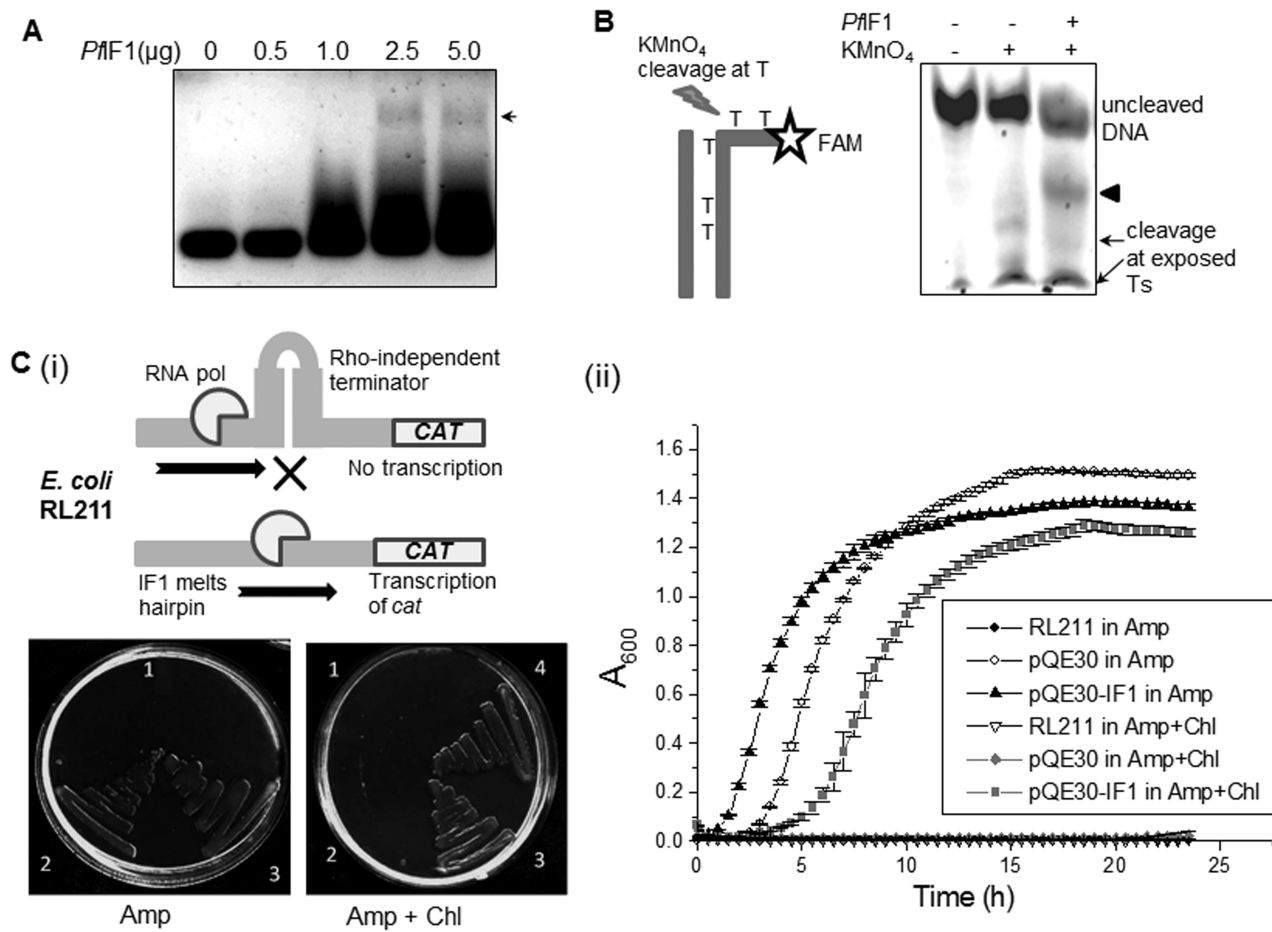


Fig. 8. *PflF1* binds and melts DNA and mediates transcription anti-termination.

A. EMSA with purified recombinant *PflF1* causes a shift in migration of the DNA probe indicating DNA binding by the protein.
 B. KMnO₄ probing of fluorescent FAM-labeled *Invertbeacon* substrate (left panel) indicates that *PflF1* has the ability to melt nucleic acids; black arrowhead indicates additional cleavage product obtained on melting of DNA in the presence of *PflF1*.
 C. *PflF1* displays transcription anti-termination activity by promoting *cat* gene transcription in the *E. coli* RL211 strain that carries a Rho-independent terminator upstream of a *cat* gene for chloramphenicol resistance. *E. coli* RL211 cells streaked on LB agar plates supplemented with ampicillin or ampicillin and chloramphenicol (panel i). 1, RL211 alone; 2, RL211 transformed with pQE30; 3 and 4, RL211 transformed with pQE30-*PflF1*. Panel ii, growth curve of different *E. coli* RL211 transformants post-induction with IPTG.

the growth curve clearly indicated that *PflF1* imparts chloramphenicol resistance [Fig. 8C (ii)] indicative of a decrease in transcription termination at the *trpL* terminator. *Plasmodium* apicoplast IF1 is thus capable of functioning as a transcription anti-terminator, probably mediated by disruption of the termination hairpin.

Discussion

Translation factors that mediate peptide chain elongation and ribosome recycling in organelles of *P. falciparum* have been previously identified and localised. Apicoplast EF-Tu is encoded by the organelle's own genome, and mitochondrial EF-Tu and a version each for EF-G and RRF have been found for the apicoplast and mitochondrion (Biswas *et al.*, 2011; Johnson *et al.*, 2011; Gupta

et al., 2013a,b). However, only a single EF-Ts-encoding gene is found on the parasite nuclear genome, and its product is targeted exclusively to the apicoplast (Biswas *et al.*, 2011). Initiation of protein synthesis in parasite organelles would contribute to regulation of gene expression and determine its fidelity and efficiency.

Among the IFs IF1, IF2 and IF3, we found that the single *P. falciparum* nuclear-encoded IF1 is an apicoplast protein. Mitochondrial translation in other organisms does not require an independent IF1 (Spencer and Spremulli, 2005) and a single IF1 probably suffices for *Plasmodium* as well (Fig. 9). Among the three putative IF2s identified, only one (IF2a, PF3D7_1312400) was an organellar protein and targeted to the mitochondrion (Fig. 9); *PflF2a* also clusters with the alveolate/kinetoplastida IF2-2_{Mit} clade in phylogenetic analysis as shown by (Atkinson *et al.*, 2012).

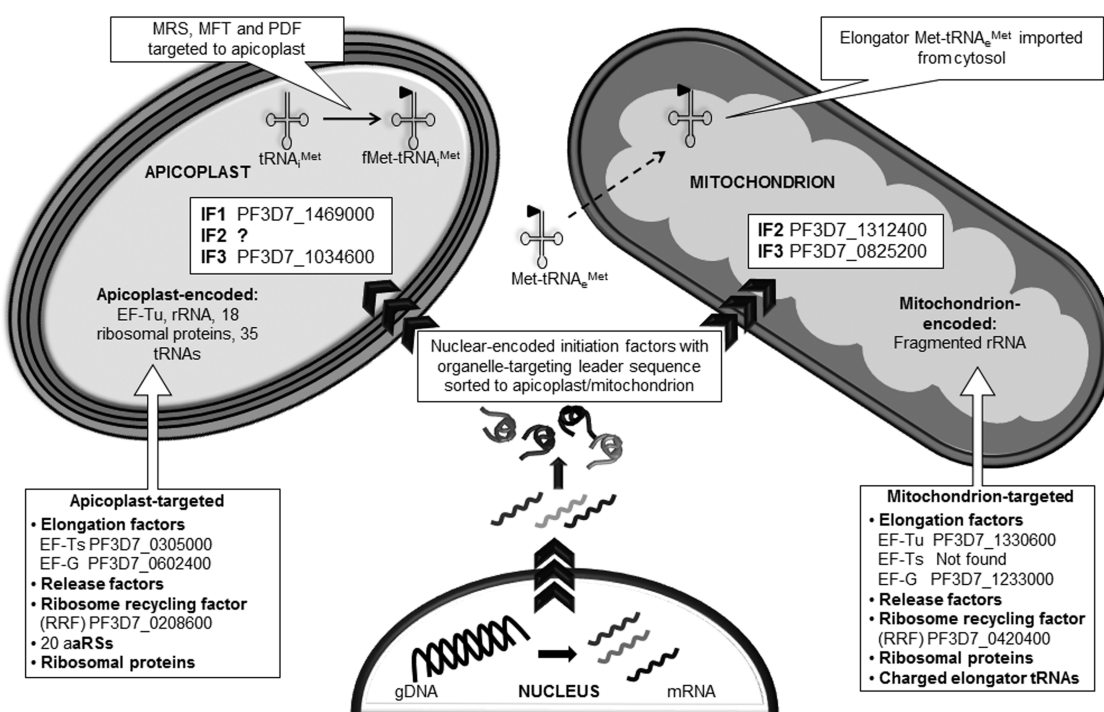


Fig. 9. Organellar distribution of translation components in *P. falciparum*. PlasmoDB IDs are provided for IFs identified in this study and elongation and recycling factors from earlier reports. The apicoplast genome encodes rRNA, 18 ribosomal proteins, 35 tRNAs and EF-Tu; the remaining components [IF1 and IF3b reported here, EF-Ts, EF-G, release factors (to be identified), RRF1, aaRSs, and remaining ribosomal proteins] of the apicoplast translation machinery are nuclear encoded. The mitochondrial genome encodes only fragmented rRNA and all other mitochondrial translation machinery components [IF2a and IF3a reported here, EF-Tu, EF-G, release factors (to be identified), RRF2, charged elongator tRNAs and ribosomal proteins] are imported by the organelle. Because the apicoplast encodes tRNA_i_{Met}, an fMet-tRNA_i_{Met} that would be formylated and deformylated by nuclear-encoded MFT and PDF, is likely to function as the initiator tRNA in the apicoplast.

Although the putative IF2b (PF3D7_0516600) was predicted to be apicoplast-targeted on the basis of its N-terminal targeting sequence, it exhibited punctate cytosolic distribution in erythrocytic parasites and did not localise to the apicoplast. This protein has previously been localised on the surface of sporozoites (Nguyen *et al.*, 2001). The third putative IF2 (IF2c, PF3D7_0827100) that has conservation of GTPase and tRNA-binding domains was also revealed to be cytosolic. Thus, an apicoplast IF2 could not be identified. Of the two putative IF3s encoded by the nuclear genome, the presence of signal and transit peptide elements in the N-terminal sequence of *Pf*F3a (PF3D7_0825200) identified it as a strong apicoplast candidate (Table 1). However, immunofluorescence assays clearly localised the protein to the mitochondrion. Although a clear mitochondrial targeting element cannot be identified in *Pf*F3a, alignment of functional domains (Fig. 1B) showed that initial prediction of an apicoplast transit peptide was erroneous as it intruded into the partial N-domain and the linker of *Pf*F3a. The other IF3 (IF3b, PF3D7_1034600), which was identifiable as an IF3 homologue only after psi-blast search and had limited identity with the factor, turned out to be an apicoplast-targeted

protein. A bipartite N-terminal targeting sequence for the apicoplast was not bioinformatically predicted for *Pf*F3b.

The OB fold, also found in *Pf*F1, is conserved in bacterial cold shock proteins (e.g. CspA and CspB) whose expression is increased during a cold shock response (Xia *et al.*, 2001). Bacterial CspS function as nucleic acid chaperones and facilitate transcription at low temperatures by destabilising RNA secondary structures. *E. coli* IF1 has been shown to similarly melt RNA secondary structures, thus influencing both transcription elongation and translation (Phadtare and Severinov, 2009). Apart from its interaction with ribosomes, a property associated with its role as a translation IF, apicoplast *Pf*F1 also exhibited nucleic acid binding and melting activities and mediated transcription anti-termination in an *E. coli* strain carrying a Rho-independent transcription terminator. This suggests a prominent ancillary function for apicoplast IF1 whereby it would help in destabilisation of DNA and RNA hairpin loops encountered during transcription and translation of the A+T rich apicoplast genome.

The identification of *Pf*F2a as the parasite mitochondrial IF2 prompted us to investigate the presence of the insertion sequence in the interdomain linker between domain V

and domain VI-C1 that was identified in IF2_{Mit} of mammalian mitochondria (Spencer and Spremulli, 2005; Gaur et al., 2008). The insertion sequence functions as an IF1 mimic and protrudes from the rest of IF2_{Mit} onto the A-site of ribosomal SSU where it interacts with conserved ribosomal elements that are known to be involved in interaction with bacterial IF1 (Yassin et al., 2011a). The sequence and size of the insertion element varies in different organisms (*B. taurus* and yeast IF2_{Mit} have 49aa and 30aa insertions respectively) and a region of low sequence conservation flanks the insertion element (Yassin et al., 2011b). ClustalW alignment of *PfIF2a* with *EclF2* and *B. taurus* IF2_{Mit} showed the presence of a corresponding 29aa insertion in the *Plasmodium* protein and structure modelling of *PfIF2a* revealed that the insertion is likely to exist as a protrusion that is partly folded as two α -helices. Thus, the *Plasmodium* mitochondrion might also overcome the absence of IF1 in the same manner as experimentally demonstrated for mammalian IF2_{Mit} (Gaur et al., 2008).

Unlike bacteria, where separate initiator and elongator tRNA^{Met} are utilised during translation, the product of a single tRNA^{Met} gene is amino-acylated and partitioned between initiation and elongation in animal mitochondria. A fraction of Met-tRNA is formylated by methionyl-tRNA-formyltransferase (MFT) and animal mitochondrial translation is initiated with a formylated Met-tRNA (fMet-tRNA). However, formylation of initiator tRNA is not essential in yeast mitochondrial translation and yeast IF2_{Mit} shows a significant degree of binding to unformylated Met-tRNA (Garofalo et al., 2003). On the other hand, bovine IF2_{Mit} has a 25-fold greater affinity for fMet-tRNA than Met-tRNA. It has been suggested that mitochondrial translation in the apicomplexan *T. gondii* uses unformylated eukaryotic elongator Met-tRNA imported from the cytosol (Pino et al., 2010). Moreover, MFT and peptide deformylase (PDF) needed for formylation of initiator tRNA and deformylation are present in single copies in the parasite nuclear genome and are targeted to the *T. gondii* apicoplast; apicoplast targeting has also been demonstrated for *P. falciparum* PDF (Tonkin et al., 2004). Our results show that mitochondrial *PfIF2a* exhibits comparable binding to formylated and unformylated *E. coli* initiator-tRNA. *PfIF2a* is thus likely to interact with unformylated elongator Met-tRNA to enable its incorporation as the peptide chain initiator loaded onto the start codon for the three *Plasmodium* mitochondrion-encoded proteins. The absence of genes encoding MFT and PDF in the apicomplexan parasites *Babesia* and *Theileria* further strengthens the view that organellar translation can proceed in the absence of formylated Met-tRNA. Our inability to identify a *P. falciparum* apicoplast IF2 leaves the issue of recruitment of initiator Met-tRNA to the start codons of apicoplast RNAs unresolved. Because an initiator tRNA^{fMet} is encoded by the *Plasmodium* apicoplast genome (Putz et al., 2010),

PDF has confirmed apicoplast localisation, and MFT is likely to be apicoplast-targeted (as in *T. gondii*), it is presumed that fMet-tRNA functions in apicoplast translation initiation. However, recruitment of this fMet-tRNA to the apicoplast translation IC would require an IF that remains to be identified. The possibility of fMet-tRNA^{fMet} transport from the apicoplast to the mitochondrion in *P. falciparum* has been proposed (Howe and Purton, 2007). This is an unlikely scenario as it would require transport of the loaded tRNA across four apicoplast and two mitochondrial membranes; deformylation of the synthesised mitochondrial protein would also remain unexplained as PDF is apicoplast targeted.

Of the distinct N-and C-domains of bacterial IF3, the C-terminal domain is capable of not only binding to the ribosome but also performing ribosome subunit dissociation and initiation fidelity functions (Petrelli et al., 2001). Although both N- and C-domains are present in *P. falciparum* apicoplast IF3b, parasite mitochondrial IF3a only has a conserved C-domain and linker with a truncated N-domain. However, recombinant *PfIF3a* that comprises the C-domain of the protein binds *E. coli* ribosomes as well as displays subunit anti-association and monosome splitting activities. Both N- and C-domains of mammalian mitochondrial IF3 contain extensions of ~30aa each that contribute to dissociation of IF3_{Mit} from mitochondrial ribosome small subunit (SSU) upon large subunit (LSU) joining (Haque et al., 2008). These extensions are not found in *PfIF3a* indicating differences from ribosomal interactions of mammalian IF3_{Mit}.

Translation regulation in yeast mitochondria employs gene-specific translation activators that interact with 5'-UTRs and ribosomes or stabilise mRNA (Fox, 1996). *Plasmodium* mitochondrial mRNA lack a Shine-Dalgarno (SD) sequence as in yeast mitochondria, but their 5'-UTRs that are too short to interact with this class of translation activators. Other activators in the form of mitochondrial membrane proteins that bind and orient mRNA into the organellar matrix face to facilitate interaction with the translation machinery (McMullin and Fox, 1993) might operate in *Plasmodium*. Trans-acting factors that direct chloroplast SD-less mRNA to ribonucleoprotein complexes are also known (Marin-Navarro et al., 2007) but whether translation initiation in the *Plasmodium* apicoplast utilises trans-activators remains to be investigated.

Reduced ribosomes of the apicoplast and mitochondrion of *Plasmodium* have lost several large and small subunit proteins accompanied by sequence and size divergences in existing ribosomal proteins (Gupta et al., 2014). This would add another level of variation in critical interactions during translation in parasite organelles. As components of the core translation apparatus required for organellar peptide chain initiation and elongation are identified, the next step is the analysis of stop codon recogni-

tion and mechanism of peptide chain termination in the *Plasmodium* apicoplast and mitochondrion. A comprehensive view of the translation process in *P. falciparum* organelles would help in understanding and evaluating target-specific effects of parasite growth inhibitory antibiotics.

Experimental procedures

Parasite culture

Plasmodium falciparum strains (3D7 and D10_{leader} ACP-GFP) were maintained using standard culturing procedures (Trager and Jensen, 1976) in human erythrocytes at 1% haematocrit in RPMI 1640 (Sigma) media supplemented with 0.5% w/v Albumax II (Life Technologies). Parasite genomic DNA was isolated by phenol-chloroform extraction, and total RNA was isolated using Trizol (Invitrogen). Superscript-III first strand synthesis kit (Invitrogen) was used for cDNA synthesis.

Identification of putative IFs and homology modelling

Putative organellar IFs were identified from the *P. falciparum* genome database (PlasmoDB) by BLAST search with bacterial IFs, followed by clustalW alignment with bacterial factors. Factors were identified by blastp except *Pf*F3b, which was identified by psi-blast. Targeting prediction softwares PlasmoAP, TargetP1.1, PATS and MitoprotII were used to predict apicoplast or mitochondrial targeting. Protein secondary structure predictions were made using Jpred3 (Cole *et al.*, 2008).

Structural modelling of the predicted organellar IFs was carried out using Modeller 9.13. PDB structures having highest identity with *Pf*IFs in BlastP were selected as template. The crystal structure of *M. tuberculosis* IF1 (PDB ID: 3I4O) (Hatzopoulos and Mueller-Dieckmann, 2010) was chosen as template for modelling *Pf*F1. For model construction, predicted mature *Pf*F1 (91–182aa) was aligned with the *Mtb*IF1 sequence using clustalW (gap open 10, gap extension 0.1). The cryo-electron microscope structure of *B. taurus* mitochondrial IF2 (*Bt*IF2_{mt}) (PDB ID: 3IZY) (Yassin *et al.*, 2011a) was taken as a template for modelling *Pf*F2a. The *Pf*F2a sequence (202–1028aa) starting from the predicted G-domain (domain IV) was aligned to the template sequence by clustalW (gap 10, gap extension 0.1). *Pf*F3a and *Pf*F3b C-domain were modelled on the crystal structure of *G. stearothermophilus* IF3 C-domain (PDB ID: 1TIG) (Biou *et al.*, 1995) as template after clustalW alignment (*Pf*F3a, 37–165aa: gap 10, gap extension 0.1; *Pf*F3b, 163–251aa: gap 25, extension 0.5) of the proteins on the template sequence. *Pf*F3b N-domain was modelled on the N-domain of *G. stearothermophilus* IF3 (PDB ID: 1TIF) (Biou *et al.*, 1995). All structure models were verified by PROCHECK. Ramachandran plots were generated on PDBsum (Laskowski, 2001) and had a high proportion of residues in the allowed regions (IF1, 100%; IF2a, 97.6%; IF3a C-domain, 99.1%; IF3b C-domain, 100%; IF3b N-domain, 97.4%). Root mean square deviation of all models was estimated by alignment with respective template structures on PyMol (Molecular Graphics System, Schrödinger, LLC).

Recombinant expression and purification of IFs

The predicted mature form (91–182aa) of putative apicoplast targeted IF1 (PF3D7_1469000), minus its apicoplast target-

ing presequence, was PCR-amplified (PCR primers in Table S1) and cloned in pQE30 for expression as an N-terminal 6xHis-tagged fusion protein. *E. coli* XL-1Blue cells transformed with pQE30-*Pf*F1 were grown in Luria Bertani (LB) medium and induced with 0.5 mM IPTG for 16 hours at 16°C. Induced cells were harvested and suspended in lysis buffer (50 mM Tris pH 8.0, 500 mM NaCl, 5% glycerol, 1 mM PMSF). *Pf*F1 was purified by Ni-NTA affinity chromatography using Ni-NTA superflow (Qiagen).

Because we could not obtain expression of the full-length gene encoding predicted mature *Pf*F3a (PF3D7_0825200), the fragment that encodes the putative ribosomal binding domain (76–165aa) was PCR-amplified from cDNA (Table S1) and cloned in pET23a for expression as a C-terminal His-tagged recombinant protein. *Pf*F3a was expressed in *E. coli* Rosetta pLysS by induction with 1 mM IPTG at 16°C for 16 hours. Cells were resuspended in lysis buffer (50 mM Tris pH 8.0, 1 M NaCl, 5 mM MgCl₂, 0.1% Triton X-100, 5% glycerol, 1 mM PMSF) and *Pf*F3a was affinity purified by Ni-NTA chromatography. Because the full-length putative organellar *Pf*F3b (PF3D7_1034600) could not be expressed, we cloned a part of the gene (encoding 43–175aa) in pET23a. Most recombinant *Pf*F3b partitioned in the insoluble fraction and *Pf*F3b inclusion bodies were used to raise antibodies in mice.

A fragment of the large IF2a gene (PF3D7_1312400) encoding the tRNA binding C-domain (IF2a-C, 639–1128aa) was PCR-amplified (Table S1) and cloned in pQE30. For *Pf*F2a-C expression, transformed *E. coli* XL-1 blue cells were induced with 1 mM IPTG at 16°C for 16 hours. Cells were lysed in lysis buffer (50 mM Tris pH 7.5, 500 mM NaCl, 5% glycerol, 1 mM NaCl), and the fusion protein was purified by Ni-NTA chromatography and dialysed in 10 kDa cutoff dialysis membrane (Sigma).

Parasite transfection

Plasmids were constructed to introduce a triple haemagglutinin tag (3× HA) at the C-termini of the endogenous loci of *Pf*F1 and *Pf*F2b [PF3D7_0516600, also called *Pf*MB2 (Nguyen *et al.*, 2001)]. These were generated by introducing a targeting region in front of the HA tags in the vector pH4A described by Triglia *et al.* (2009). In the case of the short *Pf*F1 gene, this consisted of 175 bp of the 5'-UTR, as well as 546 bp of the coding sequence. In the case of *Pf*F2b, this consisted of the 3' coding region (684 bp), which was PCR-amplified with primers containing BgIII and PstI sites (Table S1) and inserted into BgIII/PstI sites in the pH4A transfection vector. To localise *Pf*F2c (PF3D7_0827100), a GFP fusion protein expressed from an episomal plasmid was generated. A 5'-terminal region (312 bp) encoding the predicted N-terminal targeting sequence of putative organellar *Pf*F2c was PCR-amplified from parasite genomic DNA using primers containing the XbaI and XmaI sites (Table S1) and cloned in front of the GFP in the pGlux.1 transfection plasmid as described in Boddey *et al.* (2009).

In all cases, 3D7 parasites were transfected by electroporation 80–100 µg of circular DNA as described by Durasisingh *et al.* (2002). Parasites were treated with the selective agent WR99210 to select for transfectants. The parasites transfected with *Pf*F1-pHA3 and *Pf*F2b-pHA3 constructs were cycled on and off WR99210 two to three times to select stable

integrants before establishing clonal lines through limiting dilution. Expression of the IF-HA fusion protein in transfectant lines was detected by western blot.

Anti-sera generation and western blotting

Antibodies against purified recombinant proteins *PfF1*, *PfF3a* or *PfF2a-C* were generated by subcutaneous immunisation in rabbits and antibodies against *PfF3b* were raised in mice (permission for animal experiments was obtained from the Institute Animal Ethics Committee). Protein (200 µg per rabbit and 50 µg per mouse) in Freund's complete adjuvant (1:1v/v) was given as primary immunisation followed by two booster doses in incomplete adjuvant of (100 µg each for rabbit and 40 µg each for mouse). Ten days after the second booster, the animals were bled to obtain polyclonal antiserum. For western blotting to detect proteins in the parasite lysate, parasites were harvested by 0.05% saponin lysis of red blood cells (RBCs), washed with 1× PBS, suspended in PBS containing protease inhibitor cocktail (Sigma) and boiled in 1× Laemmli buffer. Western blotting was carried out using serial dilutions of antiserum as primary Ab and goat anti-rabbit/mouse HRP conjugate (Calbiochem) as secondary Ab. Signals were detected using a chemiluminiscent detection system (Millipore).

Confocal microscopy

Plasmodium falciparum-infected RBCs were fixed in PBS containing 4% (v/v) para-formaldehyde and 0.0075% (v/v) glutaraldehyde, washed in PBS and permeabilised with 0.1% (v/v) Triton X-100 in PBS for 15 minutes at room temperature as described by Tonkin *et al.* (2004). After multiple washes with PBS, cells were blocked in 3% BSA in PBS for 1 hour at 4°C and incubated overnight in primary antibodies *viz.* anti-sera against recombinant IFs (1:50) and mouse or rabbit anti-HU_p Ab (1:100) (Ram *et al.*, 2008), the latter being a marker for the apicoplast. After washing with PBS, cells were probed with Alexa Fluor 568-tagged anti-rabbit Ab and Alexa Fluor 488-tagged anti-mouse Ab (1:1000) (Invitrogen) in 3% BSA. After addition of secondary antibodies, the cells were incubated on stationary poly-L-lysine coated glass cover slips for 2 hours at room temperature. 4,6-Diamidino-2-phenylindole (DAPI) (0.2 µg ml⁻¹) was used for nuclear staining. For mitochondrial staining, cells were incubated with 50 nM Mitotracker Red CMX-ROS (Invitrogen) for 30 min at 37°C prior to fixing; anti-rabbit Alexa Fluor 514-tagged Ab or anti-mouse Alexa Fluor 488-tagged Ab were used as secondary Abs for detecting IFs in Mitotracker-stained cells. Cover slips were gently washed with PBS and mounted on anti-fade mounting media. Imaging was carried out on a Leica SP8 confocal microscope using 63X oil immersion objective.

HA-tagged *PfF1* and *PfF2b* in transfectant parasite lines were labeled using rat anti-HA monoclonal antibody 3F10 (1:100, Roche). Colocalisation experiments with mitochondrial signals were performed by labeling live parasites with 10 nM Mitotracker Red (Invitrogen), before fixing as described above. Fixed parasites were then labeled with rat anti-HA Ab and anti-rat Alexa Fluor 488-tagged Ab (Invitrogen) for 1 h at room temperature. For colocalisation with an apicoplast

marker, rabbit anti-acyl carrier protein (a kind gift from Prof. G.I. McFadden), was used and secondary detection of ACP performed with anti-rabbit Alexa Fluor 488-tagged Ab; HA was detected with anti-rat Alexa Fluor 594-tagged Ab. Cells were stained with DAPI and mounted onto slides for analysis. Microscopy was performed using an AxioPlan 2 fluorescence microscope (Zeiss) and images captured using the AxioCam MR camera and AxioVision software (Zeiss). Images were processed using ImageJ (Abramoff *et al.*, 2004).

Ribosome binding assay

Vacant *E. coli* 70S ribosomes were isolated from MRE600 strain and stored in storage buffer A [20 mM Tris pH 7.5, 10 mM magnesium acetate, 50 mM NH₄Cl, 3 mM dithiothreitol (DTT)] as described earlier (Kiel *et al.*, 2003). For separation of 30S and 50S subunits, 15 mg of 70S ribosome were dialysed against ribosome splitting buffer (Buffer S: 20 mM Tris-Cl pH 7.5, 1 mM MgCl₂, 100 mM NH₄Cl, 0.2 mM DTT) for at least 6 hours. Dialysed subunits (100 A₂₆₀) were loaded on 15–30% sucrose density gradient prepared in buffer S and centrifuged at 25 000 rpm for 16 hours in SW40 rotor (Beckman). Gradient fractions were collected, and absorbance was recorded at 254 nm. Fractions containing the 30S and 50S subunits (confirmed by SDS-PAGE) were pooled separately and pelleted by centrifugation at 45 000 rpm for 12 hours in Ti70 rotor (Beckman). Pellets were resuspended in buffer A by gentle mixing and stored at -70°C until use.

For ribosome binding assay, 30S and 50S ribosome subunits and *PfF1*, *PfF3a* or the control GST protein were incubated (ratio 1:1) in binding buffer (8 mM Tris-Cl pH 7.4, 40 mM NH₄Cl, 3.5 mM magnesium acetate, 1 mM DTT, 2.5% glycerol) for 1 hour at 30°C. The reaction mixture was then diluted to 500 µl with the reaction buffer and allowed to pass through a 100 kDa cut-off Centricon (Millipore) at 2000 × g for 15 minutes at 4°C. The filter was washed three times with 0.5 ml binding buffer. The complexes on the filter were retrieved in minimum volume of buffer (50 µl), loaded onto SDS-PAGE and visualised by Coomassie staining. IFs were detected by western blotting using anti-His antibody (1:5000).

IF3 ribosomal anti-association assay and monosome splitting

For assaying anti-association activity of *PfF3a*, *E. coli* 70S ribosomes (15 mg) were first split into constituent 50S and 30S subunits by dialysing against low Mg²⁺ Buffer S for 6 hours at 4°C. Split subunits (5 mM) were incubated with or without *PfF3a* (30 µM) at 30°C for 30 minutes after which Mg²⁺ concentration was raised to 8 mM by addition of MgCl₂. A positive control reaction was similarly set up with *EclF3* (30 µM). The reaction was further incubated for 10 minutes at 30°C and loaded on 15–30% sucrose gradient prepared in subunit re-association buffer (Buffer R: 20 mM Tris-Cl pH 7.5, 8.2 mM MgCl₂, 100 mM NH₄Cl, 0.2 mM DTT). Ultracentrifugation was carried out at 36 000 rpm for 3.5 hours at 4°C in SW40 rotor (Beckman). Gradient fractions were collected from the bottom of the tube and absorbance at 254 nm was recorded. For visualisation of subunit separation, peak fractions were separated on 12% SDS-PAGE and stained with Coomassie blue.

For assaying monosome splitting in the presence of *Pf*F3a, reactions containing 0.14 µM 70S ribosome were incubated with *Pf*F3 alone or with recombinant *Pf*EF-G_{Mit} (6 µM) and *Pf*RRF2 (6 µM) (Gupta *et al.*, 2013b) in the absence or presence of *Pf*F3 (5 µM) in Buffer R (supplemented with 250 µM GTP if *Pf*EF-G_{Mit} was added) at 30°C for 30 minutes. After incubation, reactions were loaded on 15–30% sucrose density gradient prepared in Buffer R followed by ultracentrifugation at 36 000 rpm in SW40 rotor (Beckman). Fractions were collected and analysed as above.

Nucleic acid binding and melting assay

For assaying *Pf*F2a-C interaction with tRNA, *E. coli* tRNA^{fMet} was aminoacylated and formylated using recombinant *E. coli* methionyl-tRNA synthetase (MRS) and methionyl-tRNA formyltransferase (MTF), whose expression plasmids (pET28a-EcMRS and pQE16-FMTp) were kind gifts from Dr. Lluis Ribas de Pouplana and Dr. Uttam RajBhandary respectively. Aminoacylation and formylation of *E. coli*tRNA^{fMet} was carried out as described by (Ramesh *et al.*, 1997). The *E. coli* Lys-tRNA^{Lys} used as control was prepared by aminoacylation with recombinant *Trypanosoma brucei* LysRS (gift from Dr. Lluis Ribas de Pouplana) (Español *et al.*, 2009). For electrophoretic mobility shift assay (EMSA), the *Pf*F2a-C binding reaction with Met-tRNA^{fMet}, fMet-tRNA^{fMet} or Lys-tRNA^{Lys} (5 µM) was set up in binding buffer (50 mM Tris-acetate pH 7.5, 5 mM MgCl₂, 100 mM NH₄Cl, 1 mM DTT, 0.2 mM GDP, 10 U Ribolock RNase inhibitor) in a final volume of 20 µl. After incubation of the binding reaction at room temperature for 30 minutes, samples were loaded on 1% agarose gel prepared and electrophoresed in 25 mM Tris-acetate pH 7.5 at 100 V for 30 minutes at 4°C. Gels were stained with ethidium bromide and densitometric analysis was done using Image-Quant TL software; percentage of tRNA probe shifted was plotted against concentration of IF2a-C and non-linear regression was applied to data points to generate K_D values using GraphPad Prism software.

To analyse DNA binding and DNA melting properties of *Pf*F1, a partially double-stranded fluorescence-tagged *Invertbeacon* DNA probe (with 9 bp stem and 4nt arm) was used as described by (Phadtare *et al.*, 2007). One hundred microlitres each of the oligonucleotides 5'-(6-FAM)-GTGTTTCTTG GGA-3' and 5'-TCCCAAGAA-3' were annealed in buffer (25 mM Tris pH 8.0, 100 mM NaCl), and the resultant DNA was used to assay DNA binding and DNA melting by *Pf*F1. DNA probe (0.2 µM) was incubated with increasing amounts of purified *Pf*F1 in DNA binding buffer (10 mM HEPES pH 7.5, 10 mM MgCl₂, 50 mM NaCl, 0.5 mM DTT, 1 mM EDTA, 10% glycerol) and incubated at room temperature for 15 minutes. For electrophoretic mobility shift assay (EMSA), reactions were loaded on 2% TAE-agarose gel and electrophoresed at 100 V in 1× TAE buffer at 4°C for 1 hour. Fluorescence imaging was done using ImageQuant LAS 4000 (GE Healthcare).

DNA melting activity of *Pf*F1 was assayed by probing with KMnO₄, which causes DNA breaks at exposed thymines. The exposed thymines in the *Invertbeacon* overhang would be cleaved even in the absence of melting while the internal thymines in the stem of the probe would be exposed only if there is melting. The fluorescent *Invertbeacon* probe (0.2 µM) was incubated in 10 mM potassium phosphate

buffer (pH 7.0) in the absence or presence of *Pf*F1 (30 µM) in a final reaction volume of 20 µl for 15 minutes at room temperature. This was followed by treatment with 1 mM KMnO₄ for 15 seconds at 37°C. Reactions were terminated by addition of β-mercaptoethanol (330 mM) followed by phenol extraction, ethanol precipitation and a 30 minute treatment with 10% v/v piperidine at 90°C. Reaction products were analysed by 12% urea-PAGE and imaged as above.

Transcription anti-termination activity

Escherichia coli strain RL211 (Weilbaecher *et al.*, 1994), which has a Rho-independent terminator upstream of a *cat* gene, was used to assay the transcription anti-termination activity of *Pf*F1. RL211 cells transformed with pQE30-*Pf*F1 were induced with 0.5 mM IPTG for 17 hours, streaked on LB plates containing ampicillin (50 µg ml⁻¹) and chloramphenicol (30 µg ml⁻¹) and incubated at 37°C overnight. Growth of these cells was also monitored at 37°C over a period of 24 hours post-induction using Bioscreen C (Growth Curves, USA).

Acknowledgements

We thank Prof. Robert Landick for the *E. coli* RL211 strain, Prof. Alan Cowman for the pGlux.1, Dr. Lluis Ribas de Pouplana for pET28a-EcMRS and pET30-TbKRS1, Dr. Uttam RajBhandary for pQE16-FMTp, Prof. G.J.W. Hol for the RIG plasmid and Prof. G.I. McFadden for anti-ACP antibodies. R.K. Srivastava is acknowledged for technical assistance and Rima Ray Sarkar and Kavita Singh for help with confocal microscopy. AH received scholarship from the University Grants Commission, India. This work was supported by the DST/INT/Spain/P-33/11 and the CSIR's Network project Splendid (BSC0104i) grants to SH and by an Australian National Health and Medical Research Council (NHMRC) project grant to SAR (628704). SAR is supported by a NHMRC RD Wright Biomedical Fellowship (1062504). The authors declare no conflict of interest. This is CDRI communication number 8921.

References

- Abramoff, M.D., Magalhaes, P.J., and Ram, S.J. (2004) Image processing with ImageJ. *Biophotonics Int* **11**: 36–42.
- Antoun, A., Pavlov, M.Y., Andersson, K., Tenson, T., and Ehrenberg, M. (2003) The roles of initiation factor 2 and guanosine triphosphate in initiation of protein synthesis. *EMBO J* **22**: 5593–5601.
- Atkinson, G.C., Kuzmenko, A., Kamenski, P., Vysokikh, M.Y., Lakunina, V., Tankov, S., *et al.* (2012) Evolutionary and genetic analyses of mitochondrial translation initiation factors identify the missing mitochondrial IF3 in *S. cerevisiae*. *Nucleic Acids Res* **40**: 6122–6134.
- Biou, V., Shu, F., and Ramakrishnan, V. (1995) X-ray crystallography shows that translational initiation factor IF3 consists of two compact alpha/beta domains linked by an alpha-helix. *EMBO J* **14**: 4056–4064.
- Biswas, S., Lim, E.E., Gupta, A., Saqib, U., Mir, S.S., Siddiqi, M.I., *et al.* (2011) Interaction of apicoplast-encoded elongation factor (EF) EF-Tu with nuclear-encoded EF-Ts medi-

- ates translation in the *Plasmodium falciparum* plastid. *Int J Parasitol* **41**: 417–427.
- Boddey, J.A., Moritz, R.L., Simpson, R.J., and Cowman, A.F. (2009) Role of the *Plasmodium* export element in trafficking parasite proteins to the infected erythrocyte. *Traffic* **10**: 285–299.
- Boelens, R., and Gualerzi, C.O. (2002) Structure and function of bacterial initiation factors. *Curr Protein Pept Sci* **3**: 107–119.
- Botte, C.Y., Dubar, F., McFadden, G.I., Marechal, E., and Biot, C. (2012) *Plasmodium falciparum* apicoplast drugs: targets or off-targets? *Chem Rev* **112**: 1269–1283.
- Carter, A.P., Clemons, W.M., Jr, Brodersen, D.E., Morgan-Warren, R.J., Hartsch, T., Wimberly, B.T., and Ramakrishnan, V. (2001) Crystal structure of an initiation factor bound to the 30S ribosomal subunit. *Science* **291**: 498–501.
- Chaubey, S., Kumar, A., Singh, D., and Habib, S. (2005) The apicoplast of *Plasmodium falciparum* is translationally active. *Mol Microbiol* **56**: 81–89.
- Christian, B.E., and Spremulli, L.L. (2009) Evidence for an active role of IF3mt in the initiation of translation in mammalian mitochondria. *Biochemistry* **48**: 3269–3278.
- Claros, M.G., and Vincens, P. (1996) Computational method to predict mitochondrially imported proteins and their targeting sequences. *Eur J Biochem* **241**: 779–786.
- Cole, C., Barber, J.D., and Barton, G.J. (2008) The Jpred 3 secondary structure prediction server. *Nucleic Acids Res* **36**: W197–W201.
- Croitoru, V., Semrad, K., Prenninger, S., Rajkowitsch, L., Vejen, M., Laursen, B.S., et al. (2006) RNA chaperone activity of translation initiation factor IF1. *Biochimie* **88**: 1875–1882.
- Dahl, E.L., and Rosenthal, P.J. (2008) Apicoplast translation, transcription and genome replication: targets for antimalarial antibiotics. *Trends Parasitol* **24**: 279–284.
- Dahl, E.L., Shock, J.L., Shenai, B.R., Gut, J., DeRisi, J.L., and Rosenthal, P.J. (2006) Tetracyclines specifically target the apicoplast of the malaria parasite *Plasmodium falciparum*. *Antimicrob Agents Chemother* **50**: 3124–3131.
- Dahlquist, K.D., and Puglisi, J.D. (2000) Interaction of translation initiation factor IF1 with the *E. coli* ribosomal A site. *J Mol Biol* **299**: 1–15.
- Duraisingh, M.T., Triglia, T., and Cowman, A.F. (2002) Negative selection of *Plasmodium falciparum* reveals targeted gene deletion by double crossover recombination. *Int J Parasitol* **32**: 81–89.
- Emanuelsson, O., Brunak, S., von Heijne, G., and Nielsen, H. (2007) Locating proteins in the cell using TargetP, SignalP and related tools. *Nat Protoc* **2**: 953–971.
- Español, Y., Thut, D., Schneider, A., and de Pouplana, L.R. (2009) A mechanism for functional segregation of mitochondrial and cytosolic genetic codes. *Proc Natl Acad Sci USA* **106**: 19420–19425.
- Feagin, J.E. (1992) The 6-kb element of *Plasmodium falciparum* encodes mitochondrial cytochrome genes. *Mol Biochem Parasitol* **52**: 145–148.
- Feagin, J.E., Harrell, M.I., Lee, J.C., Coe, K.J., Sands, B.H., Cannone, J.J., et al. (2012) The fragmented mitochondrial ribosomal RNAs of *Plasmodium falciparum*. *PLoS ONE* **7**: e38320.
- Foth, B.J., Ralph, S.A., Tonkin, C.J., Struck, N.S., Fraunholz, M., Roos, D.S., et al. (2003) Dissecting apicoplast targeting in the malaria parasite *Plasmodium falciparum*. *Science* **299**: 705–708.
- Fox, T.D. (1996) Translational control of endogenous and recoded nuclear genes in yeast mitochondria: regulation and membrane targeting. *Experientia* **52**: 1130–1135.
- Garcia, C., Fortier, P.L., Blanquet, S., Lallemand, J.Y., and Dardel, F. (1995a) Solution structure of the ribosome-binding domain of *E. coli* translation initiation factor IF3. Homology with the U1A protein of the eukaryotic spliceosome. *J Mol Biol* **254**: 247–259.
- Garcia, C., Fortier, P.L., Blanquet, S., Lallemand, J.Y., and Dardel, F. (1995b) 1H and 15N resonance assignments and structure of the N-terminal domain of *Escherichia coli* initiation factor 3. *Eur J Biochem* **228**: 395–402.
- Garofalo, C., Trinko, R., Kramer, G., Appling, D.R., and Hardesty, B. (2003) Purification and characterization of yeast mitochondrial initiation factor 2. *Arch Biochem Biophys* **413**: 243–252.
- Gaur, R., Grasso, D., Datta, P.P., Krishna, P.D., Das, G., Spencer, A., et al. (2008) A single mammalian mitochondrial translation initiation factor functionally replaces two bacterial factors. *Mol Cell* **29**: 180–190.
- Goodman, C.D., Su, V., and McFadden, G.I. (2007) The effects of anti-bacterials on the malaria parasite *Plasmodium falciparum*. *Mol Biochem Parasitol* **152**: 181–191.
- Grunberg-Manago, M., Dessen, P., Pantaloni, D., Godefroy-Colburn, T., Wolfe, A.D., and Dondon, J. (1975) Light-scattering studies showing the effect of initiation factors on the reversible dissociation of *Escherichia coli* ribosomes. *J Mol Biol* **94**: 461–478.
- Gualerzi, C., Risuleo, G., and Pon, C.L. (1977) Initial rate kinetic analysis of the mechanism of initiation complex formation and the role of initiation factor IF-3. *Biochemistry* **16**: 1684–1689.
- Gupta, A., Mir, S.S., Saqib, U., Biswas, S., Vaishya, S., Srivastava, K., et al. (2013a) The effect of fusidic acid on *Plasmodium falciparum* elongation factor G (EF-G). *Mol Biochem Parasitol* **192**: 39–48.
- Gupta, A., Mir, S.S., Jackson, K.E., Lim, E.E., Shah, P., Sinha, A., et al. (2013b) Recycling factors for ribosome disassembly in the apicoplast and mitochondrion of *Plasmodium falciparum*. *Mol Microbiol* **88**: 891–905.
- Gupta, A., Shah, P., Haider, A., Gupta, K., Siddiqi, M.I., Ralph, S.A., and Habib, S. (2014) Reduced ribosomes of the apicoplast and mitochondrion of *Plasmodium* spp. and predicted interactions with antibiotics. *Open Biol* **4**: 140045.
- Haque, M.E., Grasso, D., and Spremulli, L.L. (2008) The interaction of mammalian mitochondrial translational initiation factor 3 with ribosomes: evolution of terminal extensions in IF3mt. *Nucleic Acids Res* **36**: 589–597.
- Hartz, D., Binkley, J., Hollingsworth, T., and Gold, L. (1990) Domains of initiator tRNA and initiation codon crucial for initiator tRNA selection by *Escherichia coli* IF3. *Genes Dev* **4**: 1790–1800.
- Hatzopoulos, G.N., and Mueller-Dieckmann, J. (2010) Structure of translation initiation factor 1 from *Mycobacterium tuberculosis* and inferred binding to the 30S ribosomal subunit. *FEBS Lett* **584**: 1011–1015.

- Howe, C.J., and Purton, S. (2007) The little genome of apicomplexan plastids: its raison d'être and a possible explanation for the 'delayed death' phenomenon. *Protist* **158**: 121–133.
- Jackson, K.E., Habib, S., Frugier, M., Hoen, R., Khan, S., Pham, J.S., et al. (2011) Protein translation in *Plasmodium* parasites. *Trends Parasitol* **27**: 467–476.
- Johnson, R.A., McFadden, G.I., and Goodman, C.D. (2011) Characterization of two malaria parasite organelle translation elongation factor G proteins: the likely targets of the anti-malarial fusidic acid. *PLoS ONE* **6**: e20633.
- Julian, P., Milon, P., Agirrezaabala, X., Lasso, G., Gil, D., Rodnina, M.V., and Valle, M. (2011) The Cryo-EM structure of a complete 30S translation initiation complex from *Escherichia coli*. *PLoS Biol* **9**: e1001095.
- Khan, S., Garg, A., Camacho, N., Van Rooyen, J., Kumar Pole, A., Belrhali, H., et al. (2013) Structural analysis of malaria-parasite lysyl-tRNA synthetase provides a platform for drug development. *Acta Crystallogr D Biol Crystallogr* **69**: 785–795.
- Kiel, M.C., Raj, V.S., Kaji, H., and Kaji, A. (2003) Release of ribosome-bound ribosome recycling factor by elongation factor G. *J Biol Chem* **278**: 48041–48050.
- La Teana, A., Pon, C.L., and Gualerzi, C.O. (1993) Translation of mRNAs with degenerate initiation triplet AUU displays high initiation factor 2 dependence and is subject to initiation factor 3 repression. *Proc Natl Acad Sci USA* **90**: 4161–4165.
- Laskowski, R.A. (2001) PDBsum: summaries and analyses of PDB structures. *Nucleic Acids Res* **29**: 221–222.
- Laursen, B.S., Sorensen, H.P., Mortensen, K.K., and Sperling-Petersen, H.U. (2005) Initiation of protein synthesis in bacteria. *Microbiol Mol Biol Rev* **69**: 101–123.
- Lim, L., and McFadden, G.I. (2010) The evolution, metabolism and functions of the apicoplast. *Philos Trans R Soc Lond B Biol Sci* **365**: 749–763.
- McCutcheon, J.P., Agrawal, R.K., Philips, S.M., Grassucci, R.A., Gerchman, S.E., Clemons, W.M., Jr, et al. (1999) Location of translational initiation factor IF3 on the small ribosomal subunit. *Proc Natl Acad Sci USA* **96**: 4301–4306.
- McMullin, T.W., and Fox, T.D. (1993) COX3 mRNA-specific translational activator proteins are associated with the inner mitochondrial membrane in *Saccharomyces cerevisiae*. *J Biol Chem* **268**: 11737–11741.
- Marin-Navarro, J., Manuell, A.L., Wu, J., and P Mayfield, S. (2007) Chloroplast translation regulation. *Photosynth Res* **94**: 359–374.
- Nguyen, T.V., Fujioka, H., Kang, A.S., Rogers, W.O., Fidock, D.A., and James, A.A. (2001) Stage-dependent localization of a novel gene product of the malaria parasite, *Plasmodium falciparum*. *J Biol Chem* **276**: 26724–26731.
- Pavlov, M.Y., Antoun, A., Lovmar, M., and Ehrenberg, M. (2008) Complementary roles of initiation factor 1 and ribosome recycling factor in 70S ribosome splitting. *EMBO J* **27**: 1706–1717.
- Petrelli, D., LaTeana, A., Garofalo, C., Spurio, R., Pon, C.L., and Gualerzi, C.O. (2001) Translation initiation factor IF3: two domains, five functions, one mechanism? *EMBO J* **20**: 4560–4569.
- Petrelli, D., Garofalo, C., Lammi, M., Spurio, R., Pon, C.L., Gualerzi, C.O., and La Teana, A. (2003) Mapping the active sites of bacterial translation initiation factor IF3. *J Mol Biol* **331**: 541–556.
- Phadtare, S., and Severinov, K. (2009) Comparative analysis of changes in gene expression due to RNA melting activities of translation initiation factor IF1 and a cold shock protein of the CspA family. *Genes Cells* **14**: 1227–1239.
- Phadtare, S., Kazakov, T., Bubunenko, M., Court, D.L., Pestova, T., and Severinov, K. (2007) Transcription antitermination by translation initiation factor IF1. *J Bacteriol* **189**: 4087–4093.
- Pino, P., Aeby, E., Foth, B.J., Sheiner, L., Soldati, T., Schneider, A., and Soldati-Favre, D. (2010) Mitochondrial translation in absence of local tRNA aminoacylation and methionyl tRNA Met formylation in Apicomplexa. *Mol Microbiol* **76**: 706–718.
- Putz, J., Giege, R., and Florentz, C. (2010) Diversity and similarity in the tRNA world: overall view and case study on malaria-related tRNAs. *FEBS Lett* **584**: 350–358.
- Ram, E.V., Naik, R., Ganguli, M., and Habib, S. (2008) DNA organization by the apicoplast-targeted bacterial histone-like protein of *Plasmodium falciparum*. *Nucleic Acids Res* **36**: 5061–5073.
- Ramesh, V., Gite, S., Li, Y., and RajBhandary, U.L. (1997) Suppressor mutations in *Escherichia coli* methionyl-tRNA formyltransferase: role of a 16-amino acid insertion module in initiator tRNA recognition. *Proc Natl Acad Sci USA* **94**: 13524–13529.
- Schleich, T., Verwolff, G.L., and Twombly, K. (1980) A circular dichroism study of *Escherichia coli* Initiation Factor-1 binding to polynucleotides. *Biochim Biophys Acta* **609**: 313–320.
- Sette, M., van Tilborg, P., Spurio, R., Kaptein, R., Paci, M., Gualerzi, C.O., and Boelens, R. (1997) The structure of the translational initiation factor IF1 from *E. coli* contains an oligomer-binding motif. *EMBO J* **16**: 1436–1443.
- Sharma, M.R., Kaushal, P.S., Gupta, M., Banavali, N.K., and Agrawal, R.K. (2013) Insights into structural basis of mammalian mitochondrial translation. In *Translation in Mitochondria and Other Organelles*. Duchêne, A.-M. (ed.). Heidelberg: Springer Berlin, pp. 1–28.
- Singh, N.S., Das, G., Seshadri, A., Sangeetha, R., and Varshney, U. (2005) Evidence for a role of initiation factor 3 in recycling of ribosomal complexes stalled on mRNAs in *Escherichia coli*. *Nucleic Acids Res* **33**: 5591–5601.
- Spencer, A.C., and Spremulli, L.L. (2005) The interaction of mitochondrial translational initiation factor 2 with the small ribosomal subunit. *Biochim Biophys Acta* **1750**: 69–81.
- Tonkin, C.J., van Dooren, G.G., Spurck, T.P., Struck, N.S., Good, R.T., Handman, E., et al. (2004) Localization of organelar proteins in *Plasmodium falciparum* using a novel set of transfection vectors and a new immunofluorescence fixation method. *Mol Biochem Parasitol* **137**: 13–21.
- Trager, W., and Jensen, J.B. (1976) Human malaria parasites in continuous culture. *Science* **193**: 673–675.
- Triglia, T., Tham, W.H., Hodder, A., and Cowman, A.F. (2009) Reticulocyte binding protein homologues are key adhesins during erythrocyte invasion by *Plasmodium falciparum*. *Cell Microbiol* **11**: 1671–1687.

- Vaidya, A.B., and Mather, M.W. (2009) Mitochondrial evolution and functions in malaria parasites. *Annu Rev Microbiol* **63**: 249–267.
- Weilbaecher, R., Hebron, C., Feng, G., and Landick, R. (1994) Termination-altering amino acid substitutions in the beta' subunit of *Escherichia coli* RNA polymerase identify regions involved in RNA chain elongation. *Genes Dev* **8**: 2913–2927.
- Wilson, R.J., and Williamson, D.H. (1997) Extrachromosomal DNA in the Apicomplexa. *Microbiol Mol Biol Rev* **61**: 1–16.
- Xia, B., Ke, H., and Inouye, M. (2001) Acquisition of cold sensitivity by quadruple deletion of the cspA family and its suppression by PNPase S1 domain in *Escherichia coli*. *Mol Microbiol* **40**: 179–188.
- Yassin, A.S., Haque, M.E., Datta, P.P., Elmore, K., Banavali, N.K., Spremulli, L.L., and Agrawal, R.K. (2011a) Insertion domain within mammalian mitochondrial translation initiation factor 2 serves the role of eubacterial initiation factor 1. *Proc Natl Acad Sci USA* **108**: 3918–3923.
- Yassin, A.S., Agrawal, R.K., and Banavali, N.K. (2011b) Computational exploration of structural hypotheses for an additional sequence in a mammalian mitochondrial protein. *PLoS ONE* **6**: e21871.
- Zuegge, J., Ralph, S., Schmuken, M., McFadden, G.I., and Schneider, G. (2001) Deciphering apicoplast targeting signals – feature extraction from nuclear-encoded precursors of *Plasmodium falciparum* apicoplast proteins. *Gene* **280**: 19–26.

Supporting information

Additional supporting information may be found in the online version of this article at the publisher's web-site.